Atmos. Chem. Phys. Discuss., 9, 23211–23269, 2009
www.atmos-chem-phys-discuss.net/9/23211/2009/

Atmospheric Chemistry and Physics Discussions

This discussion paper is/has been under review for the journal Atmospheric Chemistry and Physics (ACP). Please refer to the corresponding final paper in ACP if available.

Winter- and summertime continental influences on tropospheric O_3 and CO observed by TES over the western North Atlantic Ocean

J. Hegarty, H. Mao, and R. Talbot

Institute for the Study of Earth, Oceans and Space, Climate Change Research Center, University of New Hampshire, Durham, New Hampshire 03824, USA

Received: 11 September 2009 – Accepted: 12 October 2009 – Published: 2 November 2009

Correspondence to: J. Hegarty (jhegarty@ccrc.sr.unh.edu)

Published by Copernicus Publications on behalf of the European Geosciences Union.

Abstract

The distribution of tropospheric O_3 and CO and the regulating factors over the western North Atlantic Ocean during winter (December, January, and February, DJF) and summer (June, July, August, JJA) were investigated using retrievals from the Tropospheric Emission Spectrometer (TES) for 2004–2006. Seasonal composites of TES retrievals, reprocessed to remove the artificial geographic and seasonal structure added from the a priori, exhibited strong seasonal differences. At the 681 hPa level during winter composite O_3 levels were uniformly low (~45 ppbv), but continental export was evident in a channel of enhanced CO (100–110 ppbv) flowing eastward from the US coast. In summer O_3 levels were variable (45–65 ppbv) and generally higher due to increased photochemical production. The main export pathway featured a channel of enhanced CO (95–105 ppbv) flowing northeastward around an anticyclone and exiting the continent over the Canadian Maritimes around 50° N. Offshore O_3-CO slopes were generally 0.15–0.20 mol mol^{-1} in JJA, indicative of photochemical O_3 production. Composites for 4 predominant circulation patterns or map types in DJF revealed that export to the lower free troposphere (681 hPa level) was enhanced by the warm conveyor belt (WCB) airstream of cyclones while stratospheric intrusions increased TES O_3 levels at 316 hPa. A major finding in the DJF data was that offshore 681 hPa CO levels behind cold fronts could be enhanced up to >150 ppbv likely by lofting from the surface via shallow convection resulting from rapid destabilization of cold air flowing over much warmer ocean waters. In JJA composites for 5 map types showed that the main export pattern of seasonal composites contained the Bermuda High as the dominate feature. However, weak cyclones and frontal troughs could enhance offshore 681 hPa CO levels to greater than 110 ppbv with O_3-CO slopes >0.50 mol mol^{-1} south of 45° N. Intense cyclones, which were not as common in the summer, enhanced export by lofting of boundary layer pollutants from over the US and also provided a possible mechanism for transporting pollutants from boreal fire outflow southward to the US east coast.

ACPD

9, 23211–23269, 2009

1 Introduction

During recent decades a number of field missions (e.g., NARE, NEAQS2002, and INTEXA/ICARTT2004) have been conducted to enhance the understanding of North American pollutant outflow (e.g., Parrish et al., 1993, 1998; Banic et al. 1996; Berkowitz et al., 1996; Cooper et al., 2001, 2002a, 2005; Fehsenfeld et al., 2006; Singh et al., 2006; Mao et al., 2006). These studies have indicated that air pollutants such as ozone (O_3) and its precursors may be lofted from the North American boundary layer in warm conveyor belts of synoptic-scale cyclones (Eckhardt et al., 2004; Creilson et al., 2003; Stohl et al., 2003) or by smaller-scale features such as sea breeze circulations (Angevine et al. 2004); and in some cases be transported by free tropospheric westerly winds over the western North Atlantic Ocean to Europe within 4–10 days (Trickl et al., 2003; Rodrigues et al., 2004; Huntrieser et al., 2005; Owen et al., 2006). They also demonstrated that stratospheric intrusions may bring O_3 and other compounds into the lower troposphere over the ocean contributing to trace gas burdens in that region (Merrill et al., 1996; Moody et al, 1996; Oltmans et al., 1996; Cooper et al., 2001, 2002b; Wotawa and Trainer, 2000; Polvani and Esler, 2007; Cammas et al., 2008). However, substantial gaps in our understanding of continental export processes remained due to the lack of long-term continuous measurements that not only covered extensive areas but also depicted the vertical structure of the atmospheric composition. To address this problem the EOS-AURA satellite was launched into a near-polar, sun-synchronous orbit on 15 July 2004 with a payload including the Tropospheric Emission Spectrometer (TES) (Schoeberl et al., 2006). TES is a Fourier transform infrared spectrometer designed to measure vertical profiles of tropospheric O_3 and its precursors such as carbon monoxide (CO) (Beer et al., 2001). These measurements may prove to be crucial for the study of many global air quality problems by providing a continuous record of tropospheric composition at several vertical levels over the multi-year lifetime of the instrument.

For our initial study on continental export using TES (Hegarty et al., 2009) we fo-

ACPD
9, 23211–23269, 2009

cused on the spring season since tropospheric O_3 levels generally peak at this time in the Northern Hemisphere and synoptic-scale circulation activity remains strong (Monks, 2000). In that study we found a strong relationship between TES O_3 and CO distributions and the highly variable circulation patterns over eastern North America and the western North Atlantic Ocean. In particular, we found enhanced O_3 and CO levels in regions of WCBs as well as evidence of tropospheric O_3 enhancements in the dry airstream (DA) regions on the western side of cyclones. These findings were consistent with previous aircraft and modeling studies and provide convincing evidence that TES measurements are capable of capturing the important variability caused by synoptic circulation systems.

In this study we extended our analysis to the winter and summer. In winter synoptic activity is strong but O_3 production is low due to the lack of solar radiation, yielding possibly overall smaller transport of O_3 compared to spring. However, during episodes of certain meteorological phenomenon such as rapidly deepening cyclonic storms known as "bombs" trans-Atlantic transport can take as little as one day. This transport occurs four times more frequent in winter than in summer (Stohl et al., 2003). Such rapid transport may be important for the budget of short-lived substances in the remote troposphere. In summer O_3 levels are high due to efficient photochemical production but synoptic cyclone activity over the mid-latitudes decreases (Monks, 2000; Zishka and Smith, 1980; Bell and Bosart, 1989; Serreze et al., 1997; Key and Chan, 1999; Owen et al., 2006). Further, impact of wild fires is often observed in summer in North American continental outflow, which can complicate quantification of anthropogenic emissions of trace gases (Honrath et al., 2004; Singh et al., 2006; Cammas et al., 2008).

In this paper we aimed to: 1) characterize the seasonal distributions of TES O_3 and CO during winter and summer over eastern North America and the western North Atlantic Ocean, and 2) examine the possible association between the variability in O_3 and CO captured in the TES observations and synoptic-scale atmospheric circulations over the northeastern US that regulate transport and dispersion of pollutants from the North

American continent. To accomplish these objectives we averaged the TES O_3 and CO retrievals during the winters (DJF) of 2005 (December 2004–February 2005) and 2006 (December 2005–February 2006) and summers (June–August, JJA) of 2005 and 2006 over a domain covering the eastern US, southeastern Canada and the adjacent Western Atlantic Ocean. Then we grouped the TES observations by synoptic circulation type and created composite O_3 and CO distributions, following Hegarty et al. (2009) and Luo et al. (2002) to identify the salient characteristics and their causal mechanisms.

2 Data

2.1 TES data

TES produces a 16-orbit Global Survey including tropospheric profiles of O_3 and CO every other day. The nadir on-the-ground footprint is ≈5.3km×8.4km with an initial along-orbit spacing between footprints of ≈544 km before that was improved to ≈182 km on 25 May 2005 after the limb scans were eliminated and replaced by an additional nadir scan (Bowman et al., 2002; Beer et al., 2001; Beer et al., 2006; Osterman et al., 2007a). Each orbit is ≈22° longitude apart. TES vertical coverage extends from 0–~33 km and in cloud-free conditions the vertical resolution is ≈6 km with sensitivity to both lower and upper troposphere as well as the stratosphere (Bowman et al., 2002; Worden et al., 2004). For this study we used the TES Level 2 V002 Global Survey data (Osterman et al., 2007b) during DJF and JJA of 2005 and 2006. Because TES generally cannot accurately measure boundary layer parameters due to a lack of thermal contrast with the surface and has approximately two degrees of freedom in the troposphere (Worden et al., 2007) we focused our attention on two levels above the boundary layer at 681 hPa and 316 hPa to represent the lower and upper free troposphere, respectively.

Atmospheric parameters are retrieved from the measured TES radiances using algorithms described by Rodgers (2000), Worden et al. (2004) and Bowman et al. (2002,

ACPD
9, 23211–23269, 2009

2006). The retrievals are mathematically constrained with a set of climatological a priori profiles, derived from MOZART simulations (Brasseur et al., 1998), representing different geographical regions and months of the year (Bowman et al., 2006). Because the geographically variable a priori adds artificial structure which can potentially obscure some of the real spatial variability, (Zhang et al., 2006) we removed this artifact by reprocessing the TES O_3 and CO profiles with a universal a priori using a procedure described in Zhang et al. (2006) and Hegarty et al. (2009). Hereafter in this study all of the TES data presented will refer to the reprocessed data.

The TES retrieval products contain diagnostic information and flags for screening out failed profiles or those with reduced sensitivity (Osterman et al., 2007a; Kulawik et al., 2006). We used the general retrieval quality flag which removes the most suspect profiles. In addition, we screened for clouds since they can impact the retrievals. Since TES sensitivity below clouds can be severely limited (Kulawik et al., 2006) we screened for clouds following Hegarty et al., (2009). We also screened for overall measurement sensitivity at the given retrieval level using the averaging kernel matrix, which is a post-processing diagnostic which defines the contribution of the each element of the true state vector to the retrieval at a particular pressure (or altitude) level. Only those profiles for which the diagonal value at the level we were examining (681 or 316 hPa) was greater than 0.01 were retained.

2.2 Meteorological analyses

We used Global Final Analysis (FNL) data from the National Centers for Environmental Prediction (NCEP) to identify the predominant atmospheric circulation patterns over eastern North America and the North Atlantic Ocean during the time period 2000–2006. FNL products are available for 4 time intervals each day (00:00, 06:00, 12:00, and 18:00 UTC) on a 1°×1° horizontal grid at the surface and 26 pressure levels vertically ranging from 1000 to 10 hPa (http://dss.ucar.edu/datasets/ds083.2).

In addition, we used HYSPLIT (Draxler and Rolph, 2003, http://www.arl.noaa.gov/ready/hysplit4.html) backward and forward trajectories, in single trajectory, ensemble,

ACPD
9, 23211–23269, 2009

and matrix mode, to aid us in determining the likely source regions for any O_3 and CO enhancements observed in the TES data downstream of North America. Rationale of the use of the use of the first two modes and details on the model input can be found in Hegarty et al. (2009). The additional matrix option enables one to automatically initiate a large number of trajectories at regular horizontal intervals. A matrix run is helpful for determining the flow into or out of an area.

Stratospheric intrusions were identified using isentropic potential vorticity (PV) from the NCAR/NCEP 2.5°×2.5° Reanalysis (NNRA, Kalnay et al., 1996). The NNRA isentropic PV analyses were available 4 times per day (00:00, 06:00, 12:00, and 18:00 UTC) at 11 isentropic levels for 270, 280, 290, 300, 315, 330, 350, 400, 450, 550, and 650 K (http://dss.ucar.edu/datasets/ds090.0). We interpolated these data to constant pressure levels to facilitate usage with NCEP FNL analyses and TES retrievals.

3 Synoptic circulation classification

Synoptic-scale circulation patterns were classified by applying the correlation-based map typing algorithm of Lund (1963) to the NCEP FNL SLP fields. We have applied this technique successfully to synoptic classification of summer- and springtime circulation patterns over the northeastern United States and the North Atlantic respectively using the NCEP grids (Hegarty et al., 2007; Hegarty et al., 2009). In brief, the algorithm calculates a correlation coefficient between the grids representing scalar meteorological analysis fields over a given spatial domain at different times. The map types are selected using a critical correlation coefficient (i.e., 0.65 for DJF and 0.70 for JJA), and then all the days in a given study period are classified as one of these types based on the degree of correlation. Typically either the sea-level pressure (SLP) or upper-level geopotential height (GPH) fields are chosen to represent the circulation patterns in the map typing algorithm. We used the SLP fields, which are usually related to the upper-level patterns and from which synoptic features can be easily identified, because the classification was more accurate compared to that based on the comparatively smooth

ACPD
9, 23211–23269, 2009

and less distinct upper-level GPH fields.

3.1 Wintertime circulation

During the study period of 2000–2006 four map types were identified for DJF (DJF1–DJF4), and five for JJA (JJA1–JJA5) as depicted in Figs. 1 and 2. The map type frequencies and the important meteorological features associated with each map type are summarized in Table 1a and b. Here we present a brief discussion of the patterns, their sequencing and how they might relate to the major hypothesized transport pathways.

The DJF circulation was characterized by periods of frequent and intense cyclonic storm activity (DJF1, DJF3, and DJF4) separated by periods of relatively calm conditions (DJF2). In the more active mode synoptic-scale cyclones tracked eastward and northeastward from southern Canada and the US (DJF3, Fig. 1c) and/or developed off the east coast and continued northeastward (DJF4, Fig. 1d). In almost all cases the cyclones exited North America as mature systems east of the Canadian Maritimes or the Labrador Coast as suggested in DJF1 (Fig. 1a), which was the most frequent map type occurring 31% of the time in winter 2005–2006 (Table 1a).

Cyclonic transport is typically presented in terms of distinct airstreams (Carlson, 1980; Cooper et al., 2001, 2002a). In the context of this study the most relevant of these would be the aforementioned warm conveyor belt (WCB) and dry airstream (DA), and the post cold front (PCF) (Parrish et al., 2000), as illustrated in Fig. 1a. The warm conveyor belt transports air masses from the boundary layer into the free troposphere along a slowly ascending north-northeastward airstream ahead of the cyclone position. In addition to the main WCB branch, a secondary branch circling to the back of the cyclone center could also be an important mechanism to transport pollutants from the urban areas on the US east coast to the lower free troposphere over the western North Atlantic. This secondary branch was identified in Cooper et al. (2002a) and denoted as W2. We also use this convention when referring to this branch. The dry airstream transports air from the upper troposphere and lower stratosphere to the

ACPD
9, 23211–23269, 2009

lower troposphere in a rapidly descending airstream spreading out behind the cyclone center. The PCF airstream descends from the middle troposphere of the northwest quadrant of the cyclone to the boundary layer behind the surface cold front and under the DA (Cooper et al., 2001, 2002a), and may be important for surface export from the immediate coastal region. These airstreams often have distinct chemical characteristics and influence the tropospheric distributions of O_3 and CO in the study domain (Merrill et al., 1996; Moody et al., 1996; Oltmans et al., 1996; Parrish et al., 2000; Cooper et al., 2002a; Owen et al., 2006; Polvani and Esler, 2007).

During the less active cyclone phase, the storm track shifted northward and the circulation was generally characterized by lighter west to southwest flow around a large anticyclone extending from the subtropical Atlantic Ocean northward into the midlatitudes as depicted in DJF2 (Fig. 1b). This map type accounted for only 14% of the classified maps in the winters of 2005 and 2006 (Table 1a) but more than half of those days (58%) were of persistent events lasting 2–3 days in a row. During these events synoptic-scale vertical transport from continental boundary layer along the US east coast was possibly restricted by the weak subsidence associated with the anticyclonic flow.

3.2 Summertime circulation

In the summer months (JJA) the circulation was dominated by a large subtropical anticyclone off the coast, usually referred to as the Bermuda High, which extended into the eastern half of the US as depicted in JJA1 (Fig. 2a). This pattern was the most frequent occurring on 28% of the days (Table 1b) and could be persistent with one event in July 2006 lasting for 8 days. It produced subsidence via light south-southwest lower tropospheric flow in much of the eastern US with generally warm and humid weather conditions. Under this general pattern, cyclones tracked north of the US-Canadian border, accompanied by trailing cold fronts that occasionally extended into the central US producing weak cyclonic flow and causing the Bermuda High to retreat offshore (i.e., JJA3 (Fig. 2c).

The second most frequent summertime pattern, JJA2, featured a cyclonic trough extending from the Labrador Peninsula southward just offshore of the northeastern US (Fig. 2b) and occurred on 17% of the days in summers 2005 and 2006 (Table 1b). During June this pattern often resulted from a well-organized cyclone that tracked northeastward from the US to the Labrador coastline. These types of systems produced well-defined cyclonic airstreams which exerted influence over the entire eastern US In contrast, later in the summer, these troughs were primarily associated with cyclones that originated in central Canada and moved eastward and southeastward. The trailing cold fronts of these systems swept southeastward and mainly influenced areas in southeastern Canada, New England, and upstate New York. Map type JJA4 shows a variation of this general pattern with the trough located further offshore and the subtropical ridge building again over the eastern US (Fig. 2d). The fact that many of the troughs seemed to weaken as they moved offshore may have accounted for the lower frequency (5%) of this map type.

Coastal cyclones, JJA5, were the least common summertime pattern occurring on only 5% of the days in summers 2005 and 2006 (Fig. 2e, Table 1b). They typically developed as migrating upper-level synoptic waves approached the coastline. However, in at least one case, on 15 June 2006, the cyclone had incorporated remnants of a tropical storm (Alberto) that had moved across the eastern Florida Panhandle two days prior (http://www.nhc.noaa.gov/pdf/TCR-AL012006_Alberto.pdf). As with east coast cyclones in other seasons the JJA5 systems produced moderately strong WCBs flowing offshore and descending DA airstreams to the west over the continent.

4 Seasonal composites of O_3 and CO distributions

For DJF the 681 hPa O_3 seasonal composite exhibited very little spatial variation with O_3 levels in most areas being near 45 ppbv (Fig. 3a), likely resulting from winter being at the minimum in the annual solar radiation cycle and therefore associated with lower photochemical production. However, the 681 hPa CO composite suggested continental

ACPD
9, 23211–23269, 2009

pollutant export to the lower free troposphere in a band of 100–110 ppbv mixing ratios extending from 30° N to 50° N along the east coast and further out to the central North Atlantic (Fig. 3b). At 316 hPa there was a steep south to north O_3 gradient with levels increasing from <50 ppbv over Florida to >150 ppbv in Canada (Fig. 3c). This strong gradient reflects the decreasing tropopause heights and increasing stratospheric influence toward the north. The 316 hPa CO composite showed very little spatial variability with most levels between 80 and 90 ppbv (Fig. 3d).

In contrast, the JJA seasonal 681 hPa O_3 composite exhibited notable spatial variability and depicted a tongue of O_3 levels >60 ppbv emanating from the east coast of the US and extending eastward into the central Atlantic (Fig. 4a). The O_3 levels decreased slightly to the south (55–60 ppbv) and more dramatically to the north with mixing ratios mostly below 50 ppbv north of 50° N. Corresponding to the greater levels of O_3 enhanced CO mixing ratios at both 681 (95–105 ppbv) and 316 hPa (CO>85 ppbv) were found to be over most of the US along an axis oriented southwest to northeast and exiting North America east of Newfoundland (Fig. 4b and d). The northward shift of this export pathway compared to winter is correlated with a northward shift in the storm track around the dominant subtropical Bermuda High as discussed in Sect. 3. While weak WCBs are likely responsible for transporting boundary layer pollutants to the lower free troposphere, the enhanced levels of CO at 316 hPa may have been made possible by rapid vertical transport in convective systems (Kiley and Fuelberg et al., 2006; Li et al., 2005; Kim et al., 2008). These possibilities are discussed in more detail in Sect. 6. The 316 hPa O_3 composite for JJA exhibited a homogeneous distribution with levels near 80 ppbv over the midlatitudes followed by a sharp increasing trend north of 50° N (Fig. 4c). The uniformity of the pattern and lack of high O_3 levels south of 50° N suggested a much decreased influence of stratospheric air as compared to winter.

To identify the possible source types of the higher O_3 and CO levels at the 681 hPa we applied the correlation of observed O_3 and CO which has been proven to be a useful diagnostic indicator of the photochemical processing of an air mass (Parrish

et al., 1993, 1998; Mao and Talbot, 2004). In export Regions 1, 2, and 3, indicated as dashed boxes in Fig. 4a, O_3 was positively correlated with CO at 681 hPa with slopes of 0.15–0.23 mol mol^{-1} at a significance level of p=0.01 (Table 2) which is close to the range of 0.2–0.35 indicted by previous in situ ground-based measurements (Parish et al., 1993, 1998; Chin et al., 1994; Mao and Talbot, 2004). Aircraft measurements during the NARE93 and ICARTT 2004 summer campaigns indicated similar slopes, which took place in the lower free troposphere just east of the North American coastline (Daum et al., 1996). However care must be taken in comparing the O_3-CO slopes to earlier studies since changing emissions of NO_x and CO in North America over time may have impacted O_3-CO slopes of anthropogenic influence (Parrish et al., 2006; Kim et al., 2006).

5 Circulation influences on O_3 and CO distributions in winter

The composite distributions of O_3 and CO for DJF exhibited notable differences between individual map types. In general, the circulation types could be grouped into 2 main types, one representing and active midlatitude storm track comprised of map types DJF1, DJF3, and DJF4, which seemed to enhance continental export, and the other for a less active midlatitude storm track, DJF2 that seemed to be less conducive to export. The differences between these groups and individual map types are discussed in the following two sections.

5.1 DJF1, DJF3, and DJF4: active midlatitude storm track

A common feature of the 681 hPa CO composites for the map types DJF1, DJF3, and DJF4 was a channel of enhanced mixing ratios >110 ppbv between 30–45° N extending eastward into the central Atlantic Ocean (Fig. 5a, c and d). This feature corresponded to the highest CO levels in the seasonal composites (Fig. 3b). For DJF3 and DJF4 the highest CO levels were generally to the east of the cyclone positions. Composite back

ACPD
9, 23211–23269, 2009

trajectories using GDAS data from the TES retrieval locations in Region 1 (Fig. 6c and d) indicated southwest to northeast flow from the continent implying that the enhanced levels were due in part to lofting of North American pollutants to the free troposphere by the WCB airstreams associated with the cyclones. This mechanism has been verified by aircraft studies of continental export (Cooper et al., 2001, 2002a; Parrish et al., 2000) and was also shown by Hegarty et al. (2009) to be a cause of enhanced lower free tropospheric O_3 and CO measured by TES east of cyclones during springtime.

The cyclones in DJF1 were centered northeast of Newfoundland (Fig. 1a), but some of the higher mixing ratios in the 681 hPa CO composite were located to the south and west of the center in a band streaming eastward from the coast line (Fig. 5a). This location is not in the main branch of the WCB and instead is located near the DA. The descending flow from the northwest indicated in the composite back trajectory plots (Fig. 6a) would work against upward transport of continental pollutants to the free troposphere and should produce lower CO levels. One possible explanation for this inconsistency is that pollutants lofted from the continent in the WCB were re-circulated to the rear of the storm in the secondary W2 branch as shown in Fig. 1a, incorporated into the subsiding DA flow and subsequently transported offshore. Another possible explanation is localized convective lofting in the PCF as proposed by Parish et al. (2000). In the case of DJF1 the PCF was located over the ocean where shallow convection in wintertime may develop due to the instability caused by cold polar or arctic continental air flowing over the relatively warm offshore waters.

We examined seven DJF1 cases that had 681 hPa CO mixing ratios >110 ppbv in two or more adjacent footprints in the offshore region of 35–45° N and west of 60° W using HYSPLIT ensemble back trajectories with EDAS meteorological data from the times and locations of the TES observations (figures not shown). One case on 26 January 2006 showed evidence of re-circulation of air to the W2 branch as a cyclone tracked over New England and into the Canadian Maritimes. A second case on 2 January 2006, had high CO mixing ratios located to the south near 35° N as a result of a WCB lofting from another approaching cyclone to the south and west of the main DJF1 cyclone.

ACPD
9, 23211–23269, 2009

Back trajectories for the remaining 5 cases all indicated descending motions from the middle and upper troposphere typical of the DA. However, satellite images and loops for these cases indicated the presence of stratocumulus cloud streets forming offshore indicative of shallow convection (Melfi et al., 1985; Etling and Brown, 1993).

Two of the 5 DA cases that had very high offshore 681 hPa CO levels (>150 ppbv) were 10 and 27 January 2006. On 10 January 2006 there were 4 CO retrievals during the 17:00 UTC overpass that ranged from 114–163 ppbv south of Nova Scotia to the western side of a cold front cloud band that coincided with an area of offshore broken clouds (Fig. 7a). These appeared as cloud streets in the 1 km GOES visible sub-image of Fig. 8. The retrieved profiles showed that the CO was enhanced from the 908 hPa to the 681 hPa level before dropping off substantially above it (Fig. 9b). The 12:00 UTC sounding out of Grey, Maine indicated a weak nocturnal inversion near the surface and a more significant subsidence inversion beginning just above the 800 hPa and extending to ≈700 hPa (Fig. 9c) which likely inhibited any upward vertical transport from the surface over the continent. However, given that the offshore sea surface temperature (shown in red on Fig. 9a) was 7°C compared to the land temperature of ≈–1°C positive sensible and latent heat fluxes from the ocean to the air may have acted to rapidly destabilize the air flowing off the continent producing convection which likely lofted some recently exported continental pollutants to higher altitudes.

On 27 January 2006 three 681 hPa CO measurements during the 06:00 UTC descending overpass ranged from 146–153 ppbv coincident with a distinct line of clouds offshore extending from southern New Jersey to the Carolinas (Fig. 9a). The 1 km GOES visible sub-image for 13:15 UTC showed that these clouds were also associated with shallow convection in organized cloud streets (Fig. 10). The vertical profile plot showed enhanced CO from the 908 hPa retrieval level up to the 422 hPa level before dropping off above it (Fig. 9b). While some of the vertical depth of this high CO feature is a result of the smoothing affect of the retrieval process, a weaker inversion (Fig. 9c) coupled with warmer ocean temperatures (~20°C) compared to the 10 January 2006 case may have enabled the convection to penetrate somewhat higher into

ACPD
9, 23211–23269, 2009

the atmosphere in some locations. However, any lofting to higher altitudes would likely increase TES sensitivity to enhanced CO due to increased thermal contrast with the relatively warmer ocean surface below and this effect on the TES CO distribution under these meteorological conditions cannot be overlooked. A possible demonstration of this is that the CO level decreased dramatically over land to the north (Fig. 9a). For example the retrieved profile at 41° N and 71° W over Rhode Island does not show any evidence of the enhancement and closely follows the shape of the universal a priori (Fig. 9b). This may be evidence that the subsidence inhibited any lofting of pollutants to altitudes to which thermal infrared instruments such as TES are less sensitive to CO (Emmons et al., 2007). To the south the profile at 25° N and 75° W which was over the ocean also showed no CO enhancement but this was possibly due to dispersion of the pollutant plume since surface winds near the Florida coast were backing to the east and while further to the northeast they remained westerly.

For both cases TES retrieved clouds with tops between 700–900 hPa, which seemed consistent with the satellite images depicting low clouds and the height of subsidence inversions indicated by sounding plots at nearby coastal locations shown in Figs. 7–10. Caution must be exercised when interpreting TES trace gas retrievals in the presence of clouds since errors in the retrievals of cloud parameters by TES can cause errors in the retrievals of trace gases (Kulawik et al., 2006; Ederling et al., 2008). However, simulations of TES retrievals have indicated that even in cloudy conditions TES has valuable skill in retrieving trace gases and that the presence of clouds will not cause systematic biases in the trace gas retrievals (Kulawik, et al., 2006). Furthermore, we did not find any bias in CO retrieval over clouds during our analysis and therefore conclude that the highly enhanced CO retrieved by TES for these two cases and others like it reflect a real trace gas feature caused by a specific set of meteorological and topographical conditions.

These cases indicate that PCF convection over the ocean enhanced by the air-ocean temperature contrast may be an important mechanism for transporting polluted air from the surface to higher altitudes. In both cases the lofting was perhaps limited to the bot-

tom of a subsidence inversion which for a time restricted flow into the free troposphere, a typical scenario for shallow convection over the ocean (Melfi et al., 1985; Babin et al., 2003; Stull, 1988). However, pollutants lofted to the upper layers of the unstable marine boundary layer (MBL) and possibly above are more accessible to WCBs of developing ocean cyclones initiated by passing upper-level baroclinic waves. In fact, model simulations by Gutowski and Jiang (1998) demonstrated that injection of moisture by shallow convection into the free troposphere is a critical factor in ocean cyclone development. Forward GDAS trajectories initiated from locations of the high TES CO retrievals at 1500 m a.s.l., which is an average of estimated MBL heights from Babin et al. (2003) and Melfi et al. (1985) and those estimated from the soundings of the two cases discussed, showed some initial descent from large-scale forcing then were incorporated into rapidly ascending airstreams within 48 h about 47% of the time. This was twice the rate as those initiated closer to the surface at 250 a.s.l. Yet, our back trajectory analysis suggests that lofting by shallow convection seems to be underrepresented in models possibly due to the coarse grid spacing of the model domain (i.e., 40 km for EDAS), which makes them unable to resolve shallow convective processes over the ocean. This further suggests that the contributions of North American continental export to pollutant levels in the lower free troposphere over the western North Atlantic Ocean may be underestimated by chemical transport models that utilize these meteorological inputs.

In contrast to the CO composites that had many enhanced features, the composite 681 hPa O_3 levels remained low (<50 ppbv) likely due to the slower photochemical production of the winter season (Fig. 11a, c and d). The exceptions were areas of O_3 levels >55 ppbv in the DJF4 composite near the North Carolina Coast and slightly less enhanced levels (50–55 ppbv) extending well offshore to 55° W (Fig. 11d). In this general region (denoted Region 1 in Fig. 11d) O_3 and CO were positively correlated (r=0.56) with a slope of 0.40 mol mol^{-1} (Fig. 12). This slope, significant at the p=0.05 significance level, was the highest of all the DJF map types in Region 1 (Table 3), is more typical of summertime suggesting a greater influence of photochemical produc-

tion than expected (Parish et al., 1993, 1998; Chin et al., 1994; Daum et al., 1996; Mao et al., 2004; Zhang et al., 2006). It probably resulted from cyclones originating at lower latitudes entraining polluted air masses that had been exposed to stronger solar radiation. The GDAS back trajectory composites shown in Fig. 6 suggest that a greater percentage of the trajectories arriving in this region passed over the Gulf of Mexico and southeastern US, at lower altitudes (typically below 700 hPa) than other map types. In addition, ensemble HYSPLIT back trajectories using EDAS data indicated that 3 of 4 DJF4 cases that featured O_3>55 ppbv in Region 1, had ensemble members that passed near or through the boundary layers (below 850 hPa) of the Gulf of Mexico, southeastern US, or southern Ohio Valley (not shown). Some of the pollutants may have undergone slow photochemical processing as they were transported further east as suggested by the O_3-CO slope of 0.49 mol mol^{-1}, significant at the p=0.01 level, for DJF1 in Region 3. This scenario is possible since the cyclones of DJF1 often represent a later stage than cyclones of DJF3.

The 316 hPa O_3 composites for both DJF4 and DJF3 (frequently preceding DJF4) indicated penetrations of enhanced O_3 (>80 ppbv) deep into the southeastern US (Fig. 13c, d). These were found to be associated with PV>1 potential vorticity unit (PVU) at 400 hPa (Fig. 14c and d) suggesting mixing of stratospheric air into the troposphere in this region (Parrish et al., 2000). It is possible that these stratospheric intrusions may have contributed to the high O_3 levels at 681 hPa for DJF4. However, we found only one case, 7 January 2006, that had enhanced O_3 and an ensemble of back trajectories from 681 hPa featuring exclusively descending motions. Other cases showed evidence of mostly ascent to 681 hPa or a mixture of ascending and descending trajectories which is consistent with the positive O_3 and CO correlation statistics and slopes for this region.

The 316 hPa CO composites for map types DJF1, DJF3, and DJF4 also showed a high degree of spatial variability (Fig. 15). However, unlike for the other composites, in many cases the locations of the enhanced CO features made it difficult to directly link them with cyclonic airstreams. One of the striking features was the high levels

ACPD
9, 23211–23269, 2009

of CO over the northeastern US and southeastern Canada for DJF4 (and to a lesser extent DJF1) which in some locations exceeded 95 ppbv. Five-day HYSPLIT ensemble back trajectories using EDAS data originating from the area of 40–55° N and 85–65° W suggested that, out of the 6 DJF4 cases, one (30 December 2005, as discussed earlier in this section) passed close to the North American boundary layer over the Gulf of Mexico States with the lowest altitude of ∼2 km. The trajectories for the other 5 cases had generally remained in the upper troposphere and lower stratosphere with Asian origin and all had passed through the Arctic at one point along the path. It is possible that the enhanced CO levels are the result of pollutants that have accumulated in the lower stratosphere as shown by Cooper et al. (2002b). In addition, aircraft and ground-based observations have shown that anthropogenic pollutants primarily from Eurasia can build up and persist in the Arctic troposphere and extend to high altitudes forming Arctic haze (Wolfsy, 1992; Law and Stohl, 2007).

5.2 DJF2: less active midlatitude storm track

In contrast to the other wintertime map types the 681 hPa CO composites for DJF2 exhibited less evidence of pollutant export to the lower free troposphere. In general, CO levels exceeding 105 ppbv were confined to the immediate US coastal areas while offshore midlatitude regions mostly exhibited levels below 100 ppbv (Fig. 5b). For DJF2 the lower tropospheric circulation pattern was dominated by a large offshore high pressure system with near zonal to west-southwest flow over the eastern US and adjacent oceans flowing anticyclonically around the high as shown in the composite of back trajectories from the TES location in Region 1 of Fig. 6b. The anticyclone produced a generally weak subsidence over the region restricting synoptic-scale vertical transport from the boundary layer over the continent. The subsidence may have been occasionally disrupted by the passage of troughs extending from cyclones tracking further north in Canada. The trajectory composites of Fig. 6b suggested incorporation of some flow from the Gulf of Mexico into the southern portion of western North Atlantic Ocean. This transport from southern regions was likely responsible for the positive O_3-CO slopes

ACPD
9, 23211–23269, 2009

(0.11 and 0.25 mol mol^{-1}) in Regions 1 and 3 (Table 3). However, given the lower CO levels off the US coast, pollutant transport to the lower free troposphere throughout most of the mid-latitudes from these systems was presumably less than that produced by the cyclones in map types DJF1, DJF3, and DJF4.

One of the only significant features of the DJF2 composites was an area of enhanced 316 hPa CO (>100 ppbv) offshore east of 55° W between 35° N and 40° N (Fig. 15b). Of nine cases that had 316 hPa CO>95 ppbv in this region, only two showed evidence of export from the North American continent based on five-day GDAS back trajectories (not shown). In the 9 December 2005 case a sharp trough on the extreme western side of the main anticyclone caused rapid uplift over the Gulf Coast States, and in the 17 December 2005 case rising motion occurred over the southeastern US on the previous day in the WCB of a DJF3 cyclone. These two cases were atypical of the DJF2 scenario as in both cases the anticyclone was not dominant and did not extend far inland allowing for export from the US via other synoptic systems.

6 Circulation influences on O_3 and CO distributions in summer

The five original map types for summer could be grouped into three more general flow patterns. The first pattern was a dominant subtropical anticyclone or Bermuda High and is represented by map types JJA1 and JJA3. The second was a cyclonic trough to the east of the northeastern US and Canadian Maritimes coastlines, shown in map types JJA2 and JJA4. The third was a closed cyclone along the east coast represented by map type JJA5. The influence of these flow patterns on the pollutant distributions will be contrasted in the following 3 sub-sections.

6.1 JJA1and JJA3: subtropical anticyclone

As discussed in Sect. 3 the dominant Bermuda High produced a general southwest to northeast flow in the lower troposphere. As a consequence the pollutant transport

ACPD
9, 23211–23269, 2009

from the continent to the free troposphere followed a northeasterly path around the western and northern edges of the anticyclone before exiting the continent east of the Canadian Maritimes. Composites of GDAS back trajectories initiated from TES observations at 681 hPa in Regions 1 and Region 2 showed this pathway as a slightly greater concentration of trajectories originating over the southeast and central US for JJA1 and JJA3 compared to the other map types (Figs. 16 and 17). This pathway was also indicated by 681 hPa TES composites which show areas of enhanced CO that dropped steeply below 95 ppbv over the ocean south of 50° N but remained at 95–105 ppbv offshore at least as far as the eastern border of the study domain at 40° W north of 50° N (Fig. 18a and c). A similar drop off in 681 hPa O_3 south of 50° N also occurred with levels decreasing from near 70 ppbv along the coast to 55–60 ppbv further offshore (Fig. 19a and c). Furthermore, for both JJA1 and JJA3 O_3-CO slopes of 0.33 and 0.18 mol mol^{-1} in Region 2, which were significant at the p=0.05 level or better, were notably greater than those in Region 1 (0.17 and 0.03 mol mol^{-1}) and Region 3 (−0.0 and −0.06 mol mol^{-1}) (Table 2). The influence of continental outflow appears to extend farther north facilitated by the circulation in these two map types.

It should be noted that direct export to the free troposphere south of 50° N was still possible by mesoscale features such as sea breeze circulations that loft pollutants from the surface that are then transported above the MBL (Li et al., 2002). This transport mechanism possibly contributed to the enhanced O_3 and CO and positive O_3-CO slopes in the western portion of Region 1. However, under this scenario it may take up to 10 days for an air parcel to cross the Atlantic Ocean (Owen et al., 2006), and subsequently the considerable photochemical aging of the air mass in transit resulted in the reduced O_3-CO slopes as observed in Region 3.

This export pattern associated with JJA1 and JJA3 appeared to be consistent throughout the troposphere as the 316 CO composites showed a high degree of spatial correlation with the 681 hPa composites (not shown). While lofting of boundary layer pollutants near the center of the anticyclone was restricted due to general subsidence, satellite images (not shown) indicated that convection near the western edge of the an-

ACPD
9, 23211–23269, 2009

ticyclone, some of which was concentrated over considerable areas in the US Central Plains and Midwest, was common and likely lofted pollutants to high altitudes in the troposphere.

6.2 JJA2 and JJA4: cyclonic trough

In contrast to JJA1 and JJA3 the cyclonic trough patterns of JJA2 and JJA4 enabled continental export south of 50° N to flow well offshore. The 681 hPa O_3 and CO composites showed enhanced levels (O_3>60 ppbv, CO>100 ppbv) south of 50° N extending to the eastern edge of the study domain at 40° W. Composite trajectories for Regions 1 and 3 (Figs. 16 and 20) showed a greater percentage of trajectories arriving from the northwest over the continent pushing pollutants to the south and east over the ocean. In addition, the O_3-CO slopes for JJA2 were 0.29 mol mol^{-1} in Region 1 and 0.57 mol mol^{-1} in Region 3, which were significant at the p=0.05 level or better, suggested that O_3 production continued in exported plumes well offshore (Table 2; Mao et al., 2006). The O_3-CO slopes for JJA4 were also high at ≈0.40 mol mol^{-1} in both regions; however, these slopes were based on 10 or fewer data points in each region and were not significant at the p=0.05 level.

There were 2 main export pathways associated with these cyclonic troughs. One was associated with the WCB which was located to the east side of the troughs. In this scenario cyclones developed over the US or along the east coast and eventually moved northeastward to Labrador lofting continental pollutants to the free troposphere in their WCBs. An analysis of the maps preceding those classified as JJA2 or JJA4 revealed that this sequence occurred about one third of the time.

The second pathway was associated with cyclones that originated in central Canada and moved eastward and southeastward with a cold frontal trough penetrating into the eastern US. The cold fronts of these systems swept southeastward and possibly produced some WCB lofting of pollutants from populated areas of eastern North America, particularly in southeastern Canada, New England, and upstate New York. In addition

ACPD
9, 23211–23269, 2009

the GDAS back trajectories into Region 3 and to a lesser extent Region 1 hint at ascent in northerly flow over the Midwest and south central plains of the US and incorporation into the upper level northwesterly flow that descends behind the cold front over the ocean (Figs. 16 and 20). During the summer it is reasonable to assume that the grid-scale ascent captured by the models may be enhanced by smaller-scale convection.

One example of this transport pattern occurred over a three-day period of 1–3 August 2006 when the circulation was classified as either JJA2 or JJA4 as a succession of troughs passed off the east coast. Satellite loops for this case indicated that large areas of convection lofted air to the free troposphere where it was transported northeastward into Canada before being incorporated into the northwesterly flow behind the cyclonic troughs and transported to the central Atlantic Ocean. The infrared (IR) image of 00:15 UTC 2 August 2006 showed an area of convection extending from the Central Plains across the upper Midwest into Canada to the west of a large anticyclone centered over the southeastern US (Fig. 21). Because of the succession of troughs during this period the enhanced O_3 and CO levels in some cases may have been associated with the northwesterly descending motion from distant sources on the back side of a trough that had previously passed as shown by the back trajectory composites of Figs. 16 and 17. However, contributions from sources along the east coast cannot be entirely dismissed since trajectories relying on meteorological data with a resolution of $1^{\circ}\times1^{\circ}$ may not have accurately resolved smaller-scale convection in this area that was evident in satellite images.

6.3 JJA5: closed east coast cyclone

It appeared that the 681 hPa O_3 and CO distributions for JJA5 were substantially influenced by the cyclonic circulation centered off the northern US east coast shown in Fig. 2c. There was an area of enhanced 681 hPa CO (>100 ppbv) extending out into the Atlantic Ocean across the entire study domain along 40° N possibly related to the WCB outflow or W2 recirculation, suggested by a few back trajectories shown in Figs 16e and 17e, as the cyclones moved up the east coast or tracked northeast-

ACPD
9, 23211–23269, 2009

ward from the central US (Fig. 18e). The 681 hPa O_3 levels in this region were also enhanced to >55 ppbv but decreased to <50 ppbv near the cyclone center (Fig. 19e), perhaps due to an increase in cloudiness, or upward transport of MBL air from relatively cleaner oceanic regions to the east of the center. In addition there were highly enhanced 681 hPa CO composite levels (115–130 ppbv) extending from central Maine southeastward into the coastal waters off southern New England. All but two of the enhanced CO measurements in this region occurred on one day following a former tropical storm traversing up the east coast.

On 14 June 2006 a very intense extratropical cyclone developed when the remnants of tropical storm Alberto combined with a migrating upper level trough over the southeastern US. Alberto had formed in the Gulf of Mexico on 11 June and made landfall along the Gulf Coast on 13 June and moved northeastward before combining with the upper level system. Individual 681 hPa CO TES retrievals of the 15 June 2006 afternoon overpass extending from southeast of Cape Cod northwestward into northern New England ranged over 112–143 ppbv. Identifying the source of pollutants for this case was challenging since back trajectories suggested a number of reasonable possibilities as indicated by the matrix plot of 4-day back trajectories using EDAS data (Fig. 22). Some pollutants originating in the boundary layer over the Gulf of Mexico, may have been incorporated into the tropical cyclone and transported northeastward with the storm while others may have been lofted from the boundary layer over the Ohio Valley and transported eastward possibly by the upper-level disturbance. In addition, there were some trajectories that had descended from the north, which when extended back in time using GDAS data to 5 days indicated ascent over the boreal forest regions of eastern Alaska (Fig. 23).

The NASA/GSFC MODIS Rapid Response System (http://rapidfire.sci.gsfc.nasa.gov/) indicated sporadic forest fires in the eastern Alaska during June of 2006 which based on the back trajectories may have contributed substantially to pollutant levels in our study region. The boreal fire season generally begins in late May and continues through summer. Fire emissions can be lofted upward as high as the lower strato-

sphere by Pyro-convective updrafts where they can be transported great distances before descending back to the lower troposphere (Wotawa and Trainer, 2001; Fromm et al., 2005; Cammas et al., 2008). It is difficult to determine the primary cause of the high CO levels observed during the 15 June 2006 case due to the complex meteorology, but it is likely that urban, industrial, and boreal forest fire sources all had substantial roles.

7 Summary

The TES free tropospheric O_3 and CO composites clearly showed enhancements downwind from North America in both DJF and JJA and that had distinct seasonal differences in their distributions. In DJF the evidence for pollutant export was primarily found in CO, as low solar insolation limited O_3 production. In JJA both CO and O_3 showed enhanced levels downwind of North America. In addition, the TES seasonal composites indicated a northward shift of the axis of greatest export from winter to summer corresponding to the northward shift of the storm track. While the a priori used in the retrieval process may add temporal and spatial structure to the retrieved distributions, the observations were reprocessed with a universal a priori to remove this artifact. Therefore the clear differences in the seasonal composites were due to real differences in trace gas distributions brought about by seasonal changes in solar insolation and circulation patterns that could be accurately sensed by TES.

In DJF the lower tropospheric CO enhancements over the western North Atlantic Ocean were due in part to lofting of pollutants from the boundary layer over North America by the WCB of passing cyclones. There was little evidence of pollutant export in the O_3 fields near the coastline due to slow photochemical production. The exception was for cyclones developing in southern latitudes that could incorporate air exposed to sunnier, warmer and more humid conditions favoring O_3 production. Enhancements to upper tropospheric O_3 during DJF were mainly due to stratospheric intrusions associated with cyclones. Enhancements to upper tropospheric CO did not appear to be

ACPD
9, 23211–23269, 2009

tied to regional circulation patterns as defined by a map type on a particular day, but resulted from long-range transport over many days. Back trajectories associated with high 316 hPa CO measurements commonly passed through the Arctic, suggesting a build-up of pollutant levels that in that region.

A potentially important finding was that CO levels over the ocean immediately downwind of the coast could be enhanced to greater than 150 ppbv behind a cold front at altitudes several kilometers above the surface. While the tropospheric flow in this region tends to be dominated by descending motions associated with the DA, shallow smaller-scale convection behind the cold front due to the rapid destabilization of cold air flowing over a relatively warm ocean surface may loft pollutants from the surface layer to at least the top of the mixed layer where it may be more readily incorporated into the free troposphere by passing baroclinic waves. This shallow convection process, typically not resolved in the back trajectory analysis due to the coarse resolution of the meteorological inputs, was associated with some of the most enhanced 681 hPa CO levels in the composites and may indicate a significant contribution to pollutant levels in the free troposphere over the western North Atlantic Ocean.

During JJA the general circulation over eastern North America and the western North Atlantic Ocean was dominated by the subtropical Bermuda High anticyclone. This pattern caused the main band of export, most evident in 681 hPa CO composites, to flow anticyclonically around the high pressure system, pass over New England, and exit the continent off the Canadian Maritime. However, weak cyclones moving northeastward across the US and those tracking across Canada with cold frontal troughs penetrating south of the US-Canadian border, exhibited enhanced O_3 and CO levels over the Atlantic Ocean south of the main seasonal export band through WCB lofting and incorporation of convectively lofted pollutants into the northwesterly flow behind preceding systems. Intense cyclonic systems were the least common circulation pattern in JJA, but also showed evidence of WCB export of both O_3 and CO. In addition, these systems can develop from combination of tropical cyclones with extra tropical systems resulting in a complex mixture of pollutants from subtropical, midlatitude urban and

ACPD
9, 23211–23269, 2009

boreal source regions.

The analysis of TES measurements in DJF and JJA presented here showed evidence of the influence of seasonal circulation patterns on pollutant levels over the western North Atlantic Ocean which was qualitatively consistent with previously studied mechanisms of continental export. At the time of the current study only 2 years of good quality TES retrievals generated with the same algorithm were available leaving gaps in data coverage that limited quantification of the contributions of various processes to export burdens. However, the demonstrated success of TES to capture major export features encourages further study using other satellite measurements, in situ observations, and models to gain a more quantitative understanding of continental export. This will add to our knowledge of its seasonal variation and climatological factors governing its contributions to the composition of the global atmosphere.

Acknowledgements. The TES Level 2 data were obtained from the NASA Langley Research Center Atmospheric Sciences Data Center (http://eosweb.larc.nasa.gov/). The GOES infrared satellite images were downloaded from the Plymouth State University Weather Center (http://vortex.plymouth.edu), and the GOES visible images were downloaded from the NOAA Comprehensive Large Array-data Stewardship System (http://www.class.ncdc.noaa.gov). The sounding plots were obtained from the University of Wyoming Department of Atmospheric Sciences (http://weather.uwyo.edu/upperair/sounding.html). The NCEP FNL and NNRA data were obtained from the NCAR Research Data Archive (http://dss.ucar.edu).

Funding for this work was provided through the NASA Earth and Space Science Fellowship Program under grant NNG05GQ30H, the New Hampshire NASA Space Grant Program under grant NNG05GG76H and by the Office of Oceanic and Atmospheric Research of the National Oceanic and Atmospheric Administration under AIRMAP grant NA06OAR4600189.

References

Angevine, W. M., Senff, C., J., White, A. B., et al.: Coastal boundary layer influence on pollutant transport in New England, J. Appl. Meteorol., 43, 1425–1437, 2004.

Babin, S. M., Sikora, T. D., and Winstead, N. S.: A case study of satellite synthetic aperture radar signatures of spatially evolving atmospheric convection over the western Atlantic Ocean, Bound.-Lay. Meteorol., 106, 527–546, 2003.
Banic, C. M., Leaitch, W. R., Isaac, G. A., Couture, M. D., Kleinman, L. I., Springston, S. R., and MacPherson, J. I.: Transport of ozone and sulfur to the North Atlantic atmosphere during the North Atlantic Regional Experiment., J. Geophys. Res., 101, 29091–29104, 1996.
Bell, G. D. and Bosart, L. F.: A 15-year climatology of Northern hemisphere closed cyclone and anticyclone centers, Mon. Weather Rev., 117, 2142–2163, 1989.
Beer, R., Glavich, T. A., and Rider, D. M.: Tropospheric Emission Spectrometer for the Earth Observing System's Aura satellite, Appl. Optics, 40, 2356–2367, 2001.
Beer, R.: TES on the Aura Mission: Scientific objectives, measurements an analysis overview, IEEE T. Geosci. Remote, 44(5), 1102–1105, 2006.
Berkowitz, C. M., Daum, P. H., Spicer, C. W., and Busness, K. M.: Synoptic patterns associated with the flux of excess ozone to the western North Atlantic, J. Geophys. Res., 101, 28923–28933, 1996.
Bowman K. W., Worden, J., Steck, T.,Worden, H. M., Clough, S., and Rodgers, C. D.: Capturing time and vertical variability of tropospheric ozone: A study using TES nadir retrievals, J. Geophys. Res., 107, doi:10.1029/2002JD002150, 2002.
Bowman, K. W., Rodgers, C. D., Kulawik, S. S., et al.: Tropospheric Emission Spectrometer Retrieval method and error analysis, IEEE T. Geosci. Remote, 44(5), 1297–1307, 2006.
Brasseur, G. P., Hauglustaine, D. A., Walters, S., et al.,: MOZART: A global chemical transport model for ozone and related chemical tracers: 1. Model description, J. Geophys. Res., 103, 28265–28289, 1998.
Cammas, J. P., Brioude, J., Chaboureau, J. P., et al.: Injection in the lower stratosphere of biomass fire emissions followed by long-range transport: a MOZAIC case study, Atmos. Chem. Phys., 95829–5846, 2009.
Carlson, T. N.: Midlatitude Weather Systems, Am. Meteorol. Soc., Boston, 507 pp., 1998.
Chin, M., Jacob, D. J., Munger, J. W., Parrish, D. D., and B. G. Doddridge: Relationship of ozone and carbon monoxide over North America, J. Geophys. Res., 99, 14 565–14 573, 1994.
Cooper, O. R., Moody, J. L., Parrish, D. D., et al.: Trace gas signatures of the airstreams within North Atlantic cyclones: Case studies from the North Atlantic Regional Experiment (NARE '97) aircraft intensive, J. Geophys. Res., 106, 5437–5456, 2001.
Cooper, O. R., Moody, J. L., Parrish, D. D., et al.: Trace gas composition of midlatitude cyclones

over the western North Atlantic Ocean: a conceptual model, J. Geophys. Res., 107, doi 10l1029/2001JD000902, 2002a.
Cooper, O. R., Moody, J. L., Parrish, D. D., et al.: Trace gas composition of mid-latitude cyclones over the western North Atlantic Ocean: A seasonal comparison of O_3 and CO, J. Geophys. Res., 107(D7), 4056, doi:10.1029/2001JD000902, 2002b.
Cooper, O. R., Stohl, A., Eckhardt, S., et al.: A springtime comparison of tropospheric ozone and transport pathways on the east and west coasts of the United States, J. Geophys. Res., 110, D05S90, doi:10.1029/2004JD005183, 2005.
Creilson, J. K., Fishman, J., and Wozniak, A. E.: Intercontinental transport of tropospheric ozone: A study of its seasonal variability across the North Atlantic utilizing tropospheric ozone residuals and its relationship to the North Atlantic Oscillation, Atmos. Chem. Phys., 3, 2053–2066, 2003, http://www.atmos-chem-phys.net/3/2053/2003/.
Daum, P. H., Kleinman, L. I., Newman, L., et al.: Chmeical and physical properties of plumes of anthropogenic pollutants transported over the North Atlantic during the North Atlantic Regional Experiment, J. Geophys. Res., 101, 29 029–29 042, 1996.
Derber, J. C., Parrish, D. F., and Lord, S. J.: The new global operational analysis system at the National Meteorological Center, Weather Forecast., 6, 538–547, 1991.
Draxler, R. R. and Rolph, G. D.: HYSPLIT (HYbrid Single-Particle Lagrangian Integrated Trajectory) Model access via NOAA ARL READY, NOAA Air Resources Laboratory, Silver Spring, MD, 2003, http://www.arl.noaa.gov/ready/hysplit4.html.
Eckhardt, S., Stohl, A., James, P., Forster, C., and Spichtinger, N.: A 15-year climatology of warm conveyor belts, J. Climate, 17, 218–236, 2004.
Ederling, A., Kulawik, S. S., Worden, J., Bowman, K., and Osterman, G.: Implementation of cloud retrievals for TES atmospheric retrievals: 2. Characterization of cloud top pressure and effective optical depth retrievals, J. Geophys, Res., 113, D16S37, doi:10.1029/2007JD008858, 2008.
Emmons, L. K., Pfister, G. G., Edwards, D. P., Gille, J. C., et al.: Measurements of Pollution in the Troposphere (MOPITT) validation exercises during summer 2004 field campaigns over North America, J. Geophys, Res., 112, D12S02, doi:10.1029/2006JD007833, 2007.
Etling, D., and Brown, R. A.: Roll vortices in the planetary boundary layer: A Review, Bound.-Lay. Meteorol., 65, 215–248, 1993.
Fehsenfeld, F. C., Ancellet, G., Bates, T. S., Goldstein, A. H., Hardesty, R. M., Honrath, R., et al.: International Consortium for Atmospheric Research on Transport and Transformation

(ICARTT): North America to Europe – Overview of the 2004 summer field study, J. Geophys. Res., 111, D23S01, doi:10.1029/2006JD007829, 2006.
Fromm, M., Belavicqua, R., Servranckx, R., Rosen, J., Thayer, J. P., Herman, J., and Larko, D.: Pyro-cumulonimbus injection of smoke to the stratosphere: observations and impact of a super blowup in northwestern Canada on 3–4 August 1998, J. Geophys. Res., 110, D08205, doi:10.1029/2004JD005350, 20827, 2005.
Gutowski, W. J. and Jiang, W.: Surface-flux regulation between cumulus convection and baroclinic waves, J. Atmos. Sci., 55, 940–953, 1998.
Hegarty J. D., Mao, H., and Talbot, R.: Synoptic controls on summertime surface ozone in the northeastern U.S., J. Geophys. Res., 112, D14306, doi:10.1029/2006JD008170, 2007.
Hegarty J. D., Mao, H., and Talbot, R.: Synoptic influences on springtime tropospheric O_3 and CO over the North American export region observed by TES, Atmos. Chem. Phys., 9, 3755–3776, 2009, http://www.atmos-chem-phys.net/9/3755/2009/.
Honrath, R. E., Owen, R. C., Val Martin, M., et al.: Regional and hemispheric impacts of anthropogenic and biomass burning emissions on summertime CO and O3 in the North Atlantic lower free troposphere, J. Geophys. Res., 109, D24310, doi:10.1029/2004JD005147, 2004.
Huntrieser, H., Heland, J., Schlager, C., et al.: Intercontinental air pollution transport from North America to Europe: Experimental evidence from airborne measurements and surface observations, J. Geophys. Res., 110, D01305, doi:10.1029/2004JD005045, 2005.
Kalnay, E., Kanamitsu, M., Kistler, W., et al.: The NCEP/NCAR 40-year reanalysis project, B. Am. Meteor. Soc., 77, 437–471, 1996.
Key, J. R. and Chan, A. C. K.: Multidecadal global and regional trends in 1000 mb and 500 mb cyclone frequencies, Geophys. Res. Lett., 26, 2053–2056, 1999.
Kiley, C. M. and Fuelberg, H. E.: An examination of summertime cyclone transport during Intercontinental Chemical Transport Experiment (INTEX-A), J. Geophys. Res., 111, doi:10.1029/2006JD007115, 2006.
Kim, S. W., Heckel, A., Mckeen, S. A., Frost, G. J., et al.: Satellite-observed US power plant NOx emission reductions and their impact on air quality, Geophysical Research Letters, 33, L22812, doi:10.1029/2006GL027749, 2006.
Kim, S. Y., Talbot, R., Mao, H., et al.: Continental outflow from the US to the upper troposphere over the North Atlantic during the NASA INTEX-NA Airborne Campaign, Atmos. Chem. Phys. 8, 1989–2005, 2008.
Kulawik, S. S., Worden, J., Eldering, A., et al.: Implementation of cloud retrievals for

Tropospheric Emission Spectrometer (TES) atmospheric retrievals: 1. Description and characterization of errors on trace gas retrievals, J. Geophys. Res., 111, D24204, doi:10.1029/2005JD006733, 2006.

Law, K. S. and Stohl, A.: Arctic air pollution: Origins and impacts, Science, 315, 1537–1540, doi:10.1126/science.1137695, 2007.

Li, Q., Jacob, D. J., Bey, I., et al.: Transatlantic transport of pollution and its effects on surface ozone in Europe and North America, J. Geophys. Res., 107(D13), 4166, doi:10.1029/2001JD001422, 2002.

Li, Q., Jacob, D. J., Rokjin, P., et al.: North American pollution outflow and the trapping of convectively lifted pollution by upper-level anticyclone, J. Geophys. Res., 110, doi:10.1029/2004JD005039, 2005.

Luo, M., Beer, R., Jacob, D. J., et al.: Simulated observation of tropospheric ozone and CO with Tropospheric Emission Spectrometer (TES) satellite instrument, J. Geophys. Res., 107, D15, doi:10.1029/2001JD000804, 2002.

Lund, I. A.: Map-pattern classification by statistical methods. J. Appl. Meterorol., 2, 56–65, 1963.

Mao, H. and Talbot, R.: O_3 and CO in New England: Temporal variations and relationships, J. Geophys. Res., 109, D21304, doi:10.1029/2004JD004913, 2004.

Mao, H., Talbot, R., Troop, D., Johnson, R., Businger, S., and Thompson, A. M.: Smart balloon observations over the North Atlantic: O3 data analysis and modeling, J. Geophys. Res., 111, D23S56, doi:10.1029/2005JD006507, 2006.

Melfi, S. H., Spinhirne, J. D., Chou, S.-H., and Palm, S. P.: Lidar observations of vertically organized convection in the planetary boundary layer over ocean, J. Clim. Appl. Meteorol., 24, 806–821, 1985.

Merrill, J. T., Moody, J. L., Oltmans, S. J., and Levy II, H.: Meteorological analysis of tropospheric ozone profiles at Bermuda, J. Geophys. Res., 101, 29 201–29 211, 1996.

Moody, J. L., Davenport, J. C., Merrill, J. T., et al.: Meteorological mechanisms for transporting O_3 over the western North Atlantic Ocean: A case study for August 24–29, 1993, J. Geophys. Res., 101, 29 213–29 277, 1996.

Monks, P. S.: A review of the observations and origins of the spring ozone maximum, Atmos. Environ., 34, 3545–3561, 2000.

Oltmans, S. J., Levy II, H., Harris, J. M., et al.: Summer and spring ozone profiles over the North Atlantic from ozonesonde measurements, J. Geophys. Res., 101, 29 179–29 200, 1996.

Osterman, G., Bowman, K. W., Eldering, A., Fisher, B., et al.: TES Level 2 (L2) Data User's Guide, Version 3.0, Jet Propulsion Laboratory, Pasadena, CA, 40 pp, http://tes.jpl.nasa.gov/uploadedfiles/TES_L2_Data_Users_Guide-1.pdf, 2007a.
Osterman, G., Bowman, K., Cady-Pereira, K., et al.: Tropospheric Emission Spectrometer (TES), validation report, JPL D#102, version 2.0, http://eosweb.larc.nasa.gov/PRODOCS/tes/validation/TESValidationReport_v2_0.pdf, 2007b.
Owen, R. C., Cooper, O. R., Stohl, A., and Honrath, R. E.: An analysis of the mechanisms of North American pollutant transport to the central North Atlantic lower free troposphere, J. Geophys. Res., 111, D23S58, doi:10.1029/2006JD007062, 2006.
Parrish, D. D., Holloway, J. S., Trainer, M., et al.: Export of North American ozone pollution to the North Atlantic Ocean, Science, 259, 1436–1439, 1993.
Parrish, D. D., Trainer, M., Holloway, J. S., et al.: Relationships between ozone and carbon monoxide at surface sites in the North Atlantic region, J. Geophys. Res., 103, 13 357–13 376, 1998.
Parrish, D. D., Holloway, J. S., Jakoubek, R., et al.: Mixing of anthropogenic pollution with stratospheric ozone: A case study from the North Atlantic wintertime troposphere, J. Geophys. Res., 105, 24 363–24 374, 2000.
Parrish, D. D.: Critical Evaluation of US on-road vehicle emission inventories, Atmos. Environ., 40(13), 2288–2300, doi:10.1016/j.atmosenv.2005.11.033, 2006.
Polvani, L. M. and Esler, J. G.: Transport and mixing of chemical air masses in idealized baroclinic life cycles, J. Geophys. Res., 112, D23102, doi:10.1029/2007JD008555, 2007.
Rodgers, C. D.: Inverse Methods for Atmospheric Sounding: Theory and Practice, World Sci., Hackensack, N.J., 2000.
Rodrigues, S., Torres, C., Guerra, J.-C., and Cuevas, E.: Transport pathways of ozone to marine and free-troposphere sites in Tenerife, Canary Islands, Atmos. Environ., 38, 4733–4747, 2004.
Schoeberl, M. R.: Overview of the EOS Aura mission, IEEE T. Geosci. Remote., 44(5), 1066–1074, 2006.
Serreze, M. C., Carse, F., Barry, R. G., and Rogers, J. C.: Icelandic low cyclone activity: Climatological features, linkages with the NAO, and relationships with recent changes in the Northern Hemisphere circulation, J. Climate, 10, 453–464, 1997.
Singh, H. B., Brune, W. H., Crawford, J. H., Jacob, D. J., and Russell, P. B.: Overview of the summer 2004 International Chemical Transport Experiment- North America (INTEX-A), J.

Geophys. Res., 111, D23S02, doi:10.1029/2006JD007905, 2006.
Stohl, A., Huntrieser, H., Richter, A., et al.: Rapid intercontinental air pollution transport associated with a meteorological bomb, Atmos. Chem. Phys., 3, 969–985, 2003, http://www.atmos-chem-phys.net/3/969/2003/.
Trickl, T., Cooper, O. R., Holger, E., et al.: Intercontinental transport and its influence on the ozone concentrations over Europe: Three case studies, J. Geophys. Res., 108, D12, 8530, doi:10.1029/2002JD002735, 2003.
Wotawa, G. and Trainer, M.: The influence of Canadian forest fires on pollutant concentrations in the United States, Science, 288, 324–328, 2000.
Worden, J., Kulawik, S. S., Shephard, M. W., et al.: Predicted errors of Tropospheric Emission Spectrometer nadir retrievals from spectral window selection, J. Geophys. Res., 109, D09308, doi:10.1029/2004JD004522, 2004.
Worden, J., Liu, X., Bowman, K., et al.: Improved tropospheric ozone profile retrievals using OMI and TES radiances, Geophys. Res. Let., 34, L01809, doi:10.1029/2006GL027806, 2007.
Zhang, L., Jacob, D. J., Bowman, K. W., et al.: Ozone-CO correlations determined by the TES satellite instrument in continental outflow regions, and prospects in synoptic climatology, J. Geophys. Res., 33., L18804, doi:10.1029/2006GL026399, 2006.
Zishka, K. M., and Smith, P. J.: The climatology of cyclones and anticyclones over North America and surrounding ocean environs for January and July, 1950–77, Mon. Weather Rev., 108, 387–401, 1980.

Table 1a. DJF map types and meteorological characteristics. Frequencies are for the winters of December 2004–February 2005 (2005), and December 2005–February 2006.

Map Type	2005–2006 Frequency (%)	Characteristics
DJF1	31	– Mature Cyclone exiting North America near Canadian Maritimes – Subsiding northwest flow around back of cyclone center covering much of northeastern US and southeastern Canada
DJF2	14	– Large oceanic anticyclone – Primarily west to southwest flow over much of eastern North America – Major storm track shifted northward
DJF3	11	– Continental cyclone – Southerly flow and rising motion over much of east coast in the WCB
DJF4	7	– Coastal cyclone – Primarily developing along the coast of the southeastern US and moving rapidly to the northeast – Rising motion and southerly flow over the southeastern US extending out into the Atlantic in the WCB – Northerly descending flow over inland after cyclone passage DA

ACPD

9, 23211–23269, 2009

Table 1b. JJA map types and meteorological characteristics.

Map Type	2005–2006 Frequency (%)	Characteristics
JJA1	28	– Subtropical anticyclone (Bermuda High) – May persist up to 8 days – Weak south and southwesterly flow and subsidence over northeastern US – Isolated rising motion associated with localized convection
JJA2	17	– Low pressure trough off immediate coast – Subsiding north-northwest DA flow along coast of northeastern US and southeastern Canadian coast, – Rising motion in WCB offshore – anticyclonic ridge rebuilding inland
JJA3	11	– Subtropical (Bermuda High) with approaching low or frontal trough inland – Southerly and southwesterly flow in eastern US and southeastern Canada.
JJA4	5	– Low pressure trough well offshore – Subtropical anticyclone re-established inland – WCB well offshore – Weak southwesterly flow around anticyclone over eastern US – Subsiding northwesterly flow in DA just east and south of Nova Scotia and Newfoundland
JJA5	5	– Coastal cyclone – WCB flow to the east of Newfoundland and – Northwesterly flow of secondary re-circulating WCB or DA over the north-eastern US

ACPD

9, 23211–23269, 2009

Table 2. JJA O_3-CO slope (mol mol^{-1}), correlation coefficient (r) and sample size (N) for circulation types in the three regions shown in Fig. 4a. The superscripts a and b indicate slope significance at the p=0.01, and 0.05 levels, respectively.

	Region 1	Region 2	Region 3
All	0.15[a] (0.20) N=253	0.20[a] (0.31) N=141	0.18[a] (0.23) N=213
JJA1	0.17[b] (0.21) N=91	0.33[a] (0.51) N=34	0.00 (0.0) N=82
JJA2	0.29[b] (0.32) N=46	0.13 (0.28) N=23	0.57[a] (0.66) N=38
JJA3	0.03 (0.04) N=29	0.18[b] (0.48) N=18	−0.06 (−0.13) N=16
JJA4	0.42 (0.46) N=9	0.34 (0.31) N=12	0.37 (0.46) N=10
JJA5	0.33 (0.48) N=12	0.02 (0.06) N=3	0.0 (−0.01) N=6

ACPD
9, 23211–23269, 2009

Table 3. DJF O_3-CO slope (mol mol^{-1}), correlation coefficient (r) and sample size (N) for circulation types in the three regions shown in Fig. 4a. The superscripts a and b indicate slope significance at the p=0.01 and 0.05 levels, respectively.

	Region 1	Region 2	Region 3
All	0.09[b] (0.18) N=188	−0.06 (−0.14) N=62	0.23[a] (0.46) N=109
DJF1	0.03 (0.09) N=52	−0.10 (−0.21) N=22	0.49[a] (0.72) N=26
DJF2	0.11 (0.20) N=53	−0.10 (−0.33) N=6	0.25[a] (0.55) N=22
DJF3	0.13 (0.23) N=15	−0.04 (−0.41) N=4	0.13 (0.37) N=18
DJF4	0.40[b] (0.56) N=16	0, 0 N=1	0.25 (0.49) N=9

ACPD
9, 23211–23269, 2009

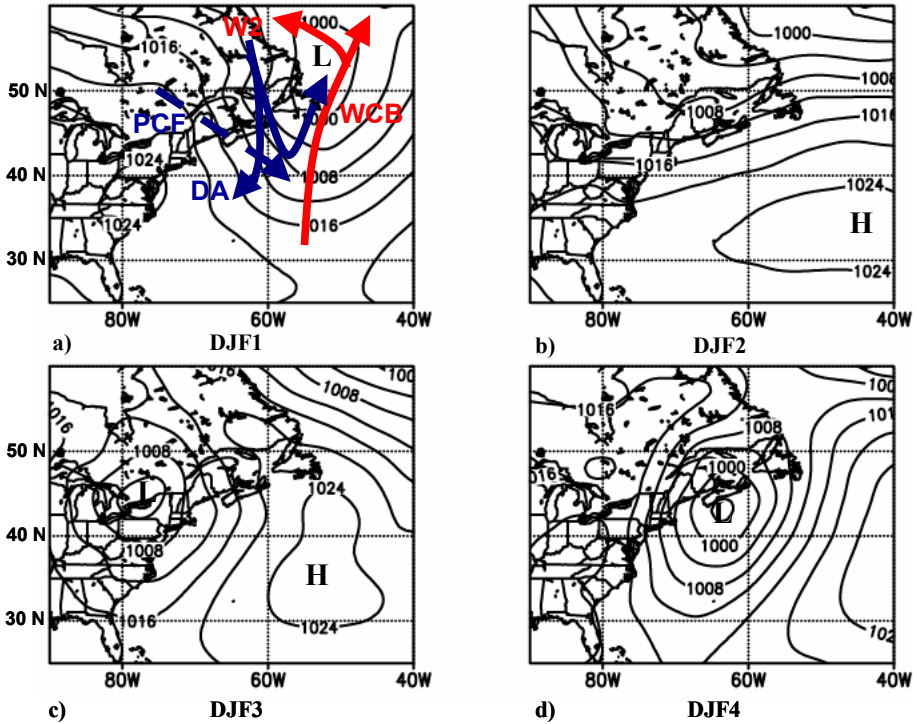

Fig. 1. Mean sea level pressure (SLP) (hPa) analyses for DJF map types DJF1–DJF4 **(a–d)** during 2005 and 2006.

ACPD

9, 23211–23269, 2009

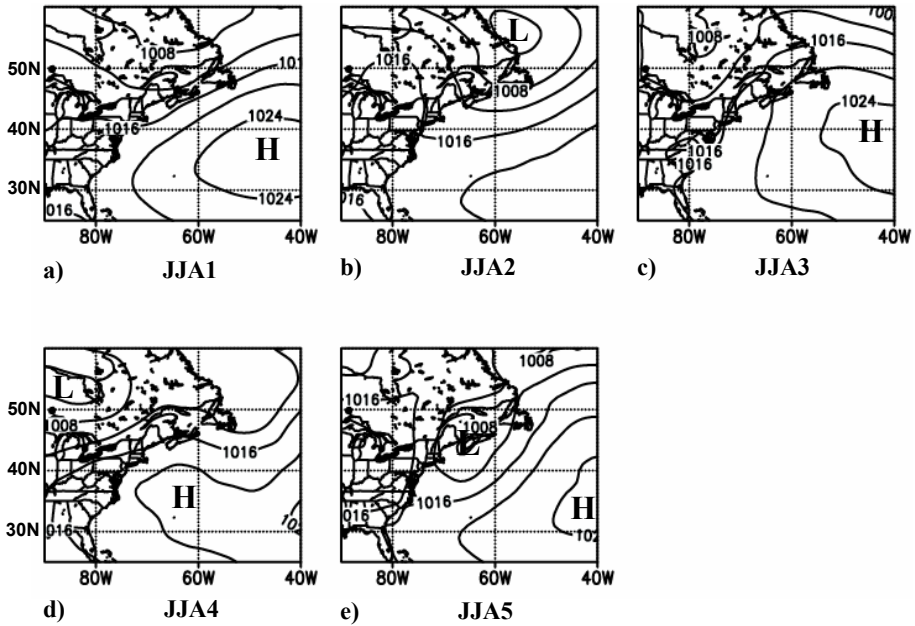

Fig. 2. Mean sea level pressure (SLP) (hPa) analyses for JJA map types JJA1–JJA2 **(a–d)** during 2005 and 2006.

ACPD
9, 23211–23269, 2009

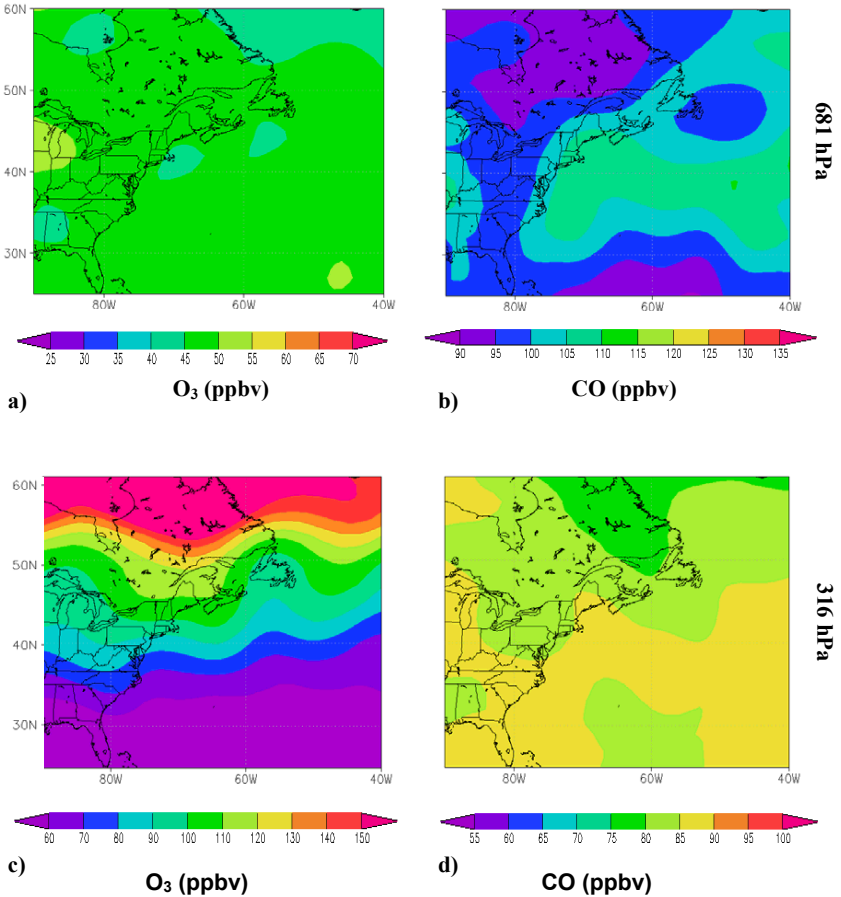

Fig. 3. The DJF seasonal composites for **(a)** 681 hPa O_3 (ppbv) **(b)** 681 hPa CO (ppbv), **(c)** 316 hPa O_3 (ppbv) and **(d)** 316 hPa CO (ppbv).

ACPD
9, 23211–23269, 2009

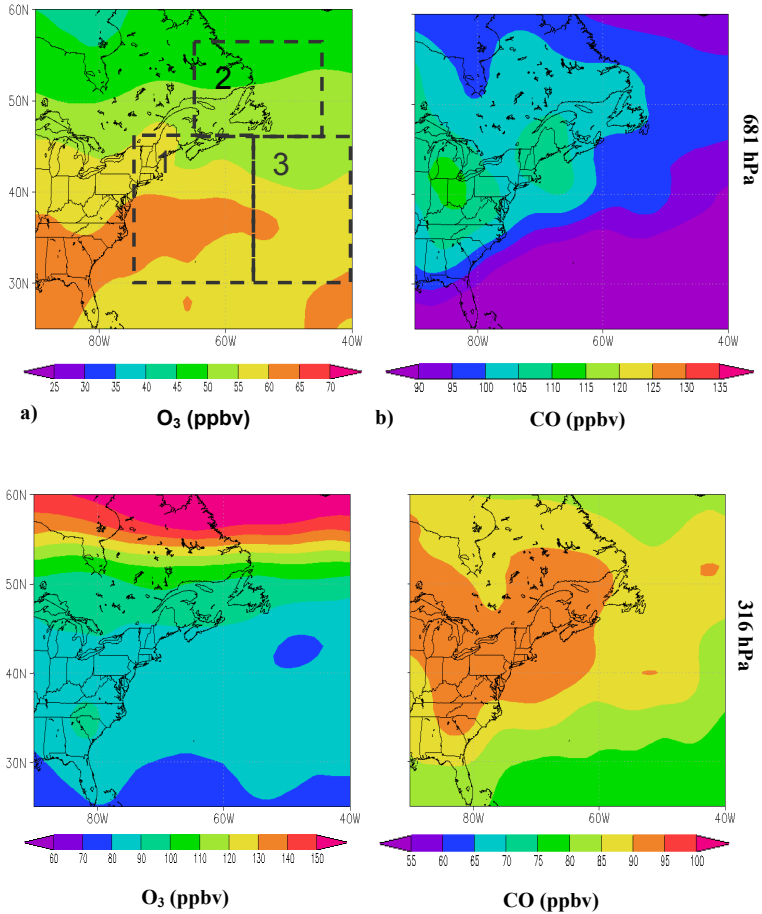

Fig. 4. The JJA seasonal composites for **(a)** 681 hPa O_3 (ppbv) **(b)** 681 hPa CO (ppbv), **(c)** 316 hPa O_3 (ppbv) and **(d)** 316 hPa CO (ppbv). Regions 1, 2, and 3 are marked as dashed black lines on (a).

ACPD
9, 23211–23269, 2009

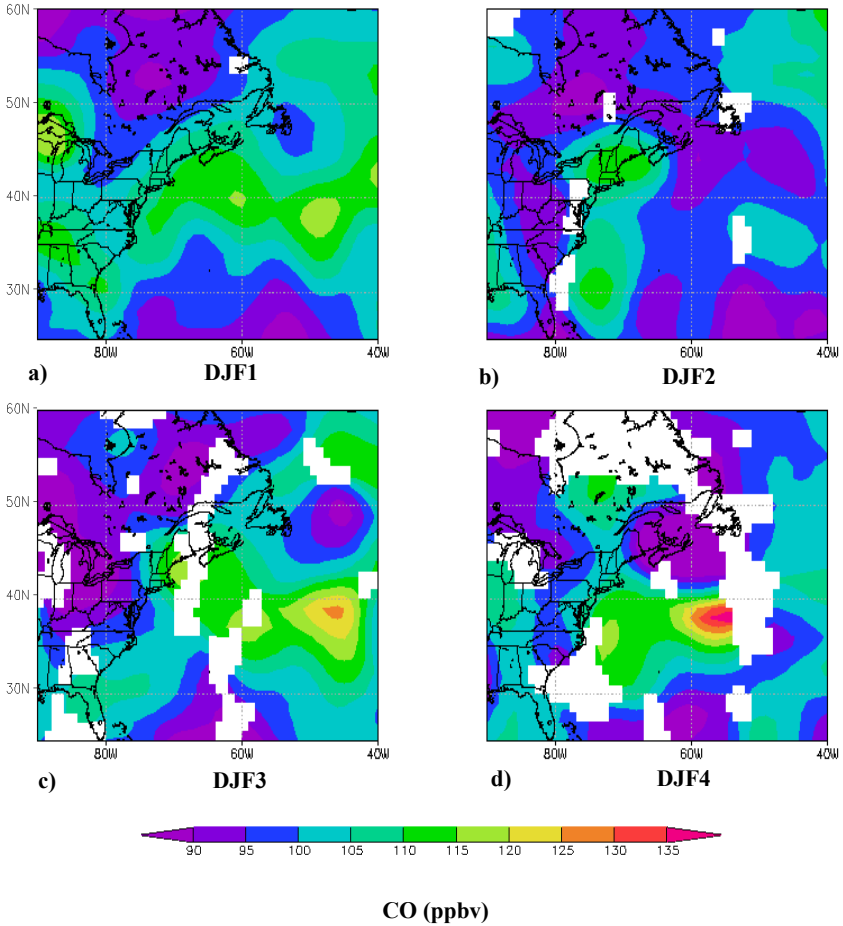

Fig. 5. The DJF 681 hPa CO (ppbv) composites for map types DJF1-DJF4 **(a–d)**.

ACPD
9, 23211–23269, 2009

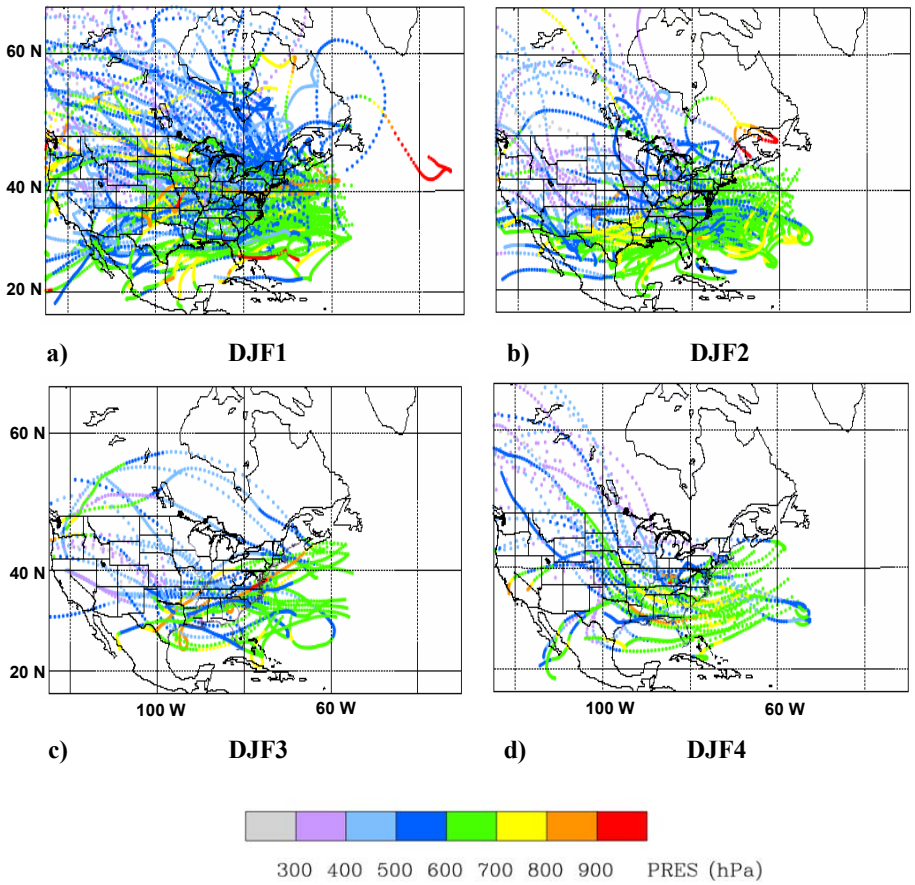

Fig. 6. Four-day HYSPLIT back trajectories using GDAS 1°×1° data from locations of TES 681 hPa observations in Region 1 for map types DJF1-DJF4 **(a–d)**. The colors indicate the pressure altitude (hPa) of the trajectory parcels.

ACPD
9, 23211–23269, 2009

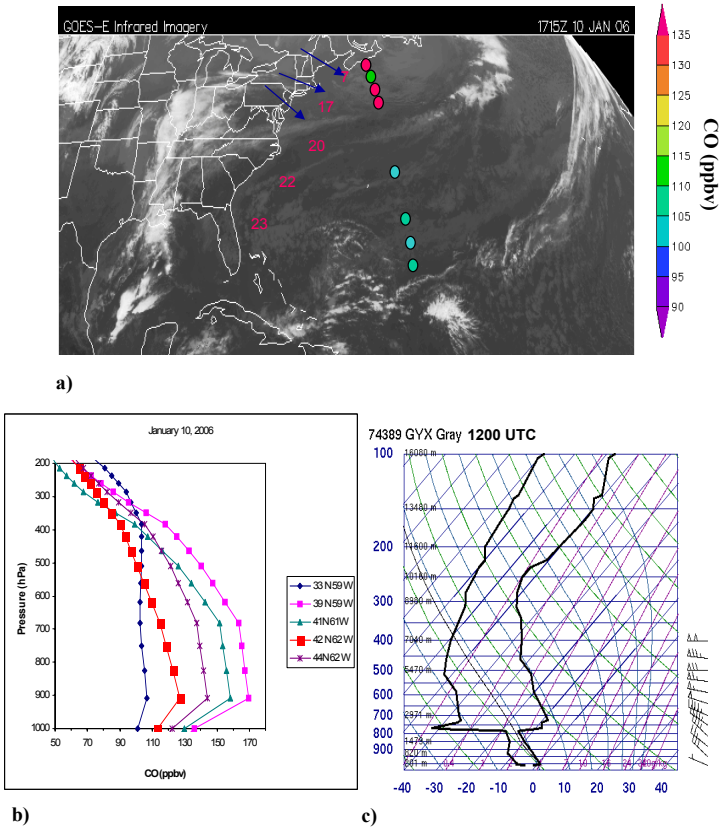

Fig. 7. Surface level CO export case on 10 January 2006, **(a)** GOES-East IR satellite image for 17:15 UTC with TES 681 hPa CO (ppbv) plotted in colored dots **(b)** TES CO retrieved profiles (ppbv) for 17:00 UTC ascending orbit, and **(c)** Skew-T sounding plot from Grey, ME for 12:00 UTC. The blue arrows on (a) show the orientation of surface streamlines and sea surface temperatures from buoy measurements are indicated with red numbers.

ACPD
9, 23211–23269, 2009

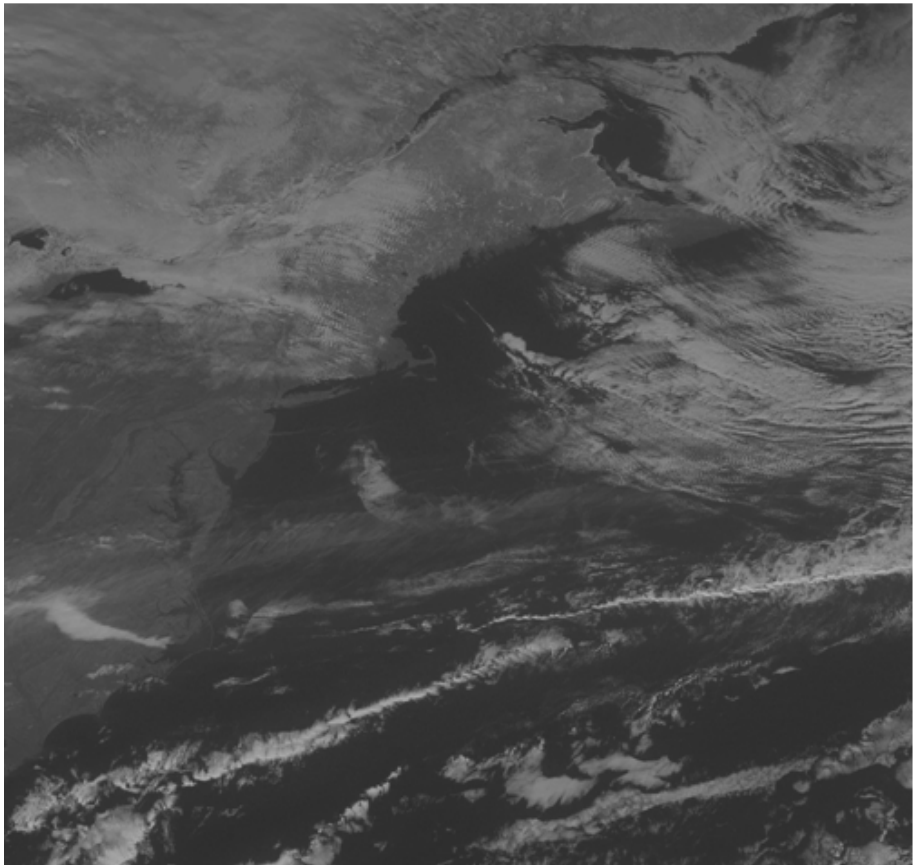

Fig. 8. GOES-East visible 1 km satellite image for 17:15 UTC 10 January 2006.

ACPD

9, 23211–23269, 2009

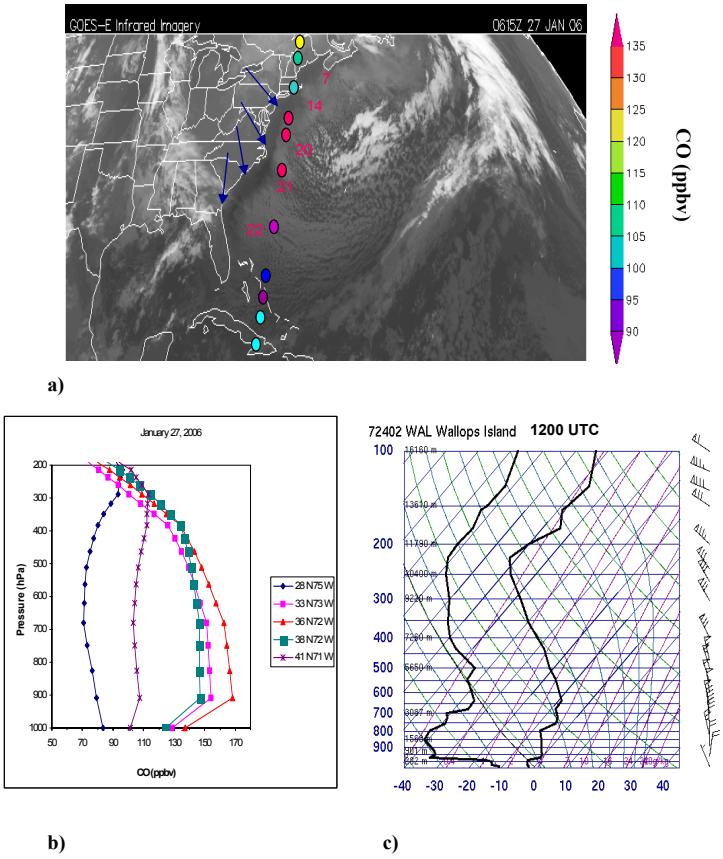

Fig. 9. Surface level CO export case on 27 January 2006, **(a)** GOES-East IR satellite image for 06:15 UTC with TES 681 hPa CO (ppbv) plotted in colored dots **(b)** TES CO retrieved profiles (ppbv) for 06:00 UTC ascending orbit, and **(c)** Skew-T sounding plot from Grey, ME for 12:00 UTC. The blue arrows on (a) show the orientation of surface streamlines and sea surface temperatures from buoy measurements are indicated with red numbers.

ACPD
9, 23211–23269, 2009

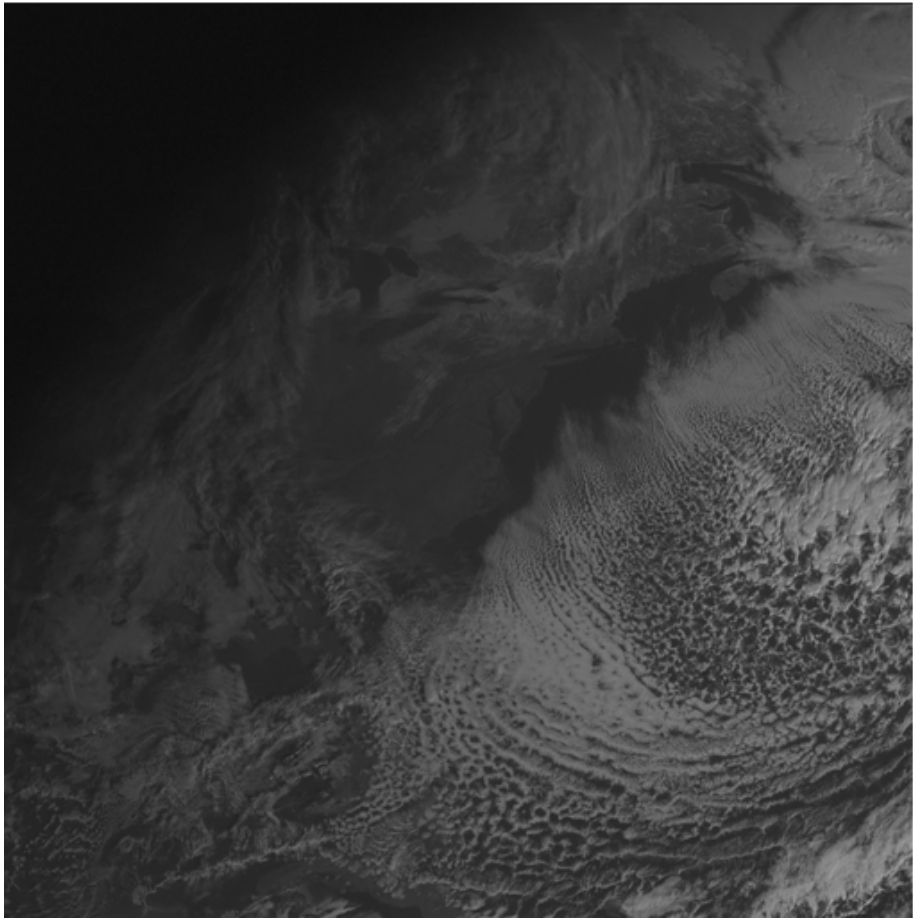

Fig. 10. GOES-East visible, 1 km satellite image for 13:31 UTC 27 January 2006.

ACPD

9, 23211–23269, 2009

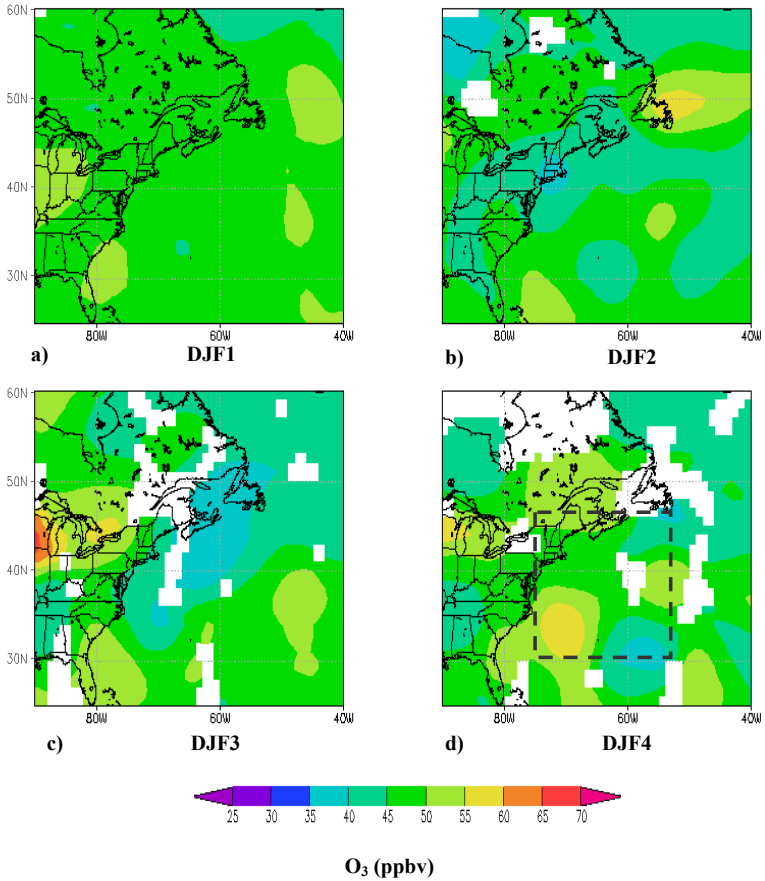

Fig. 11. The DJF 681 hPa O_3 (ppbv) composites for the map types DJF1–DJF4 **(a–d)**. Region 1, represented in the scatter plot of Fig. 12, is marked as a dashed line on (d).

ACPD
9, 23211–23269, 2009

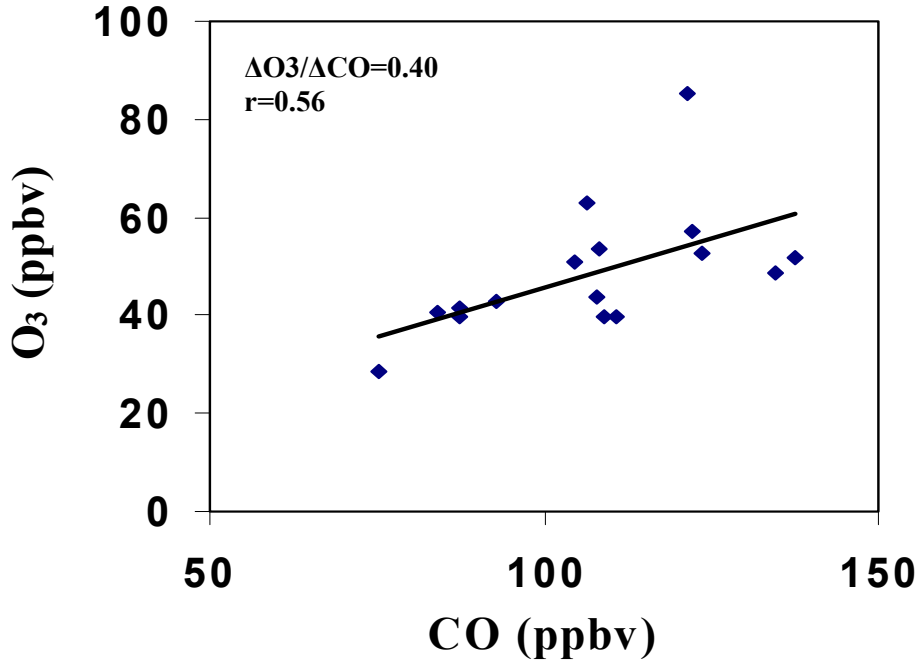

Fig. 12. Scatter plot of 681 hPa O_3 versus CO in Region 1 for DJF4.

ACPD
9, 23211–23269, 2009

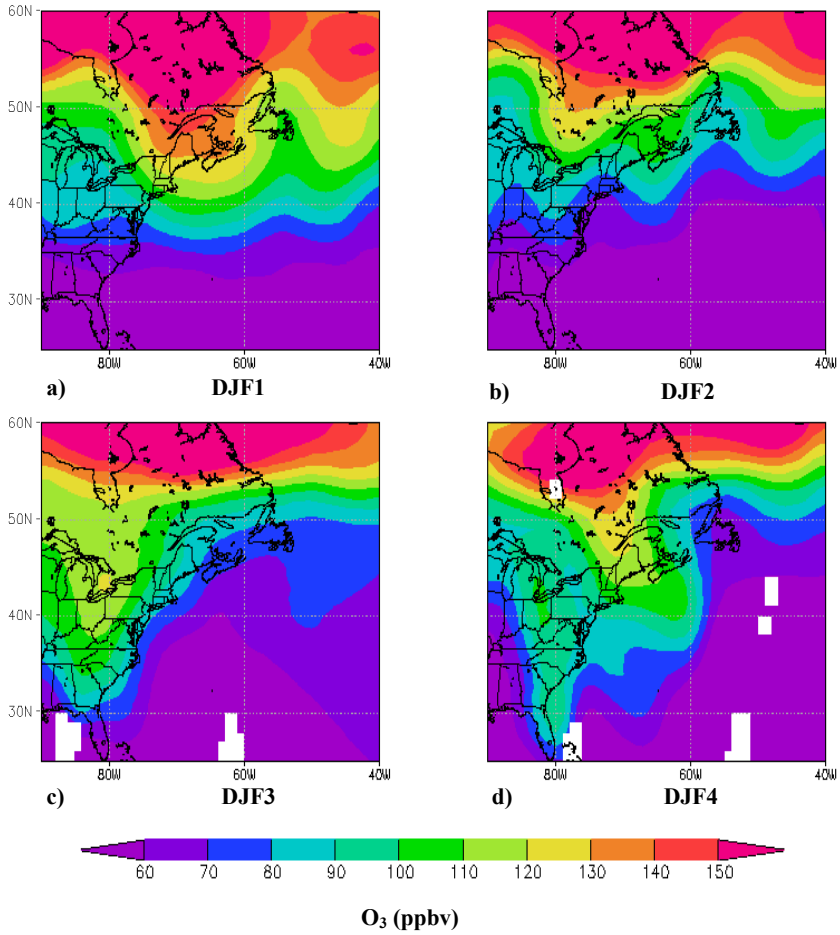

Fig. 13. The DJF 316 hPa O_3 (ppbv) composites for map types DFJ1–DFJ4 **(a–d)**.

ACPD
9, 23211–23269, 2009

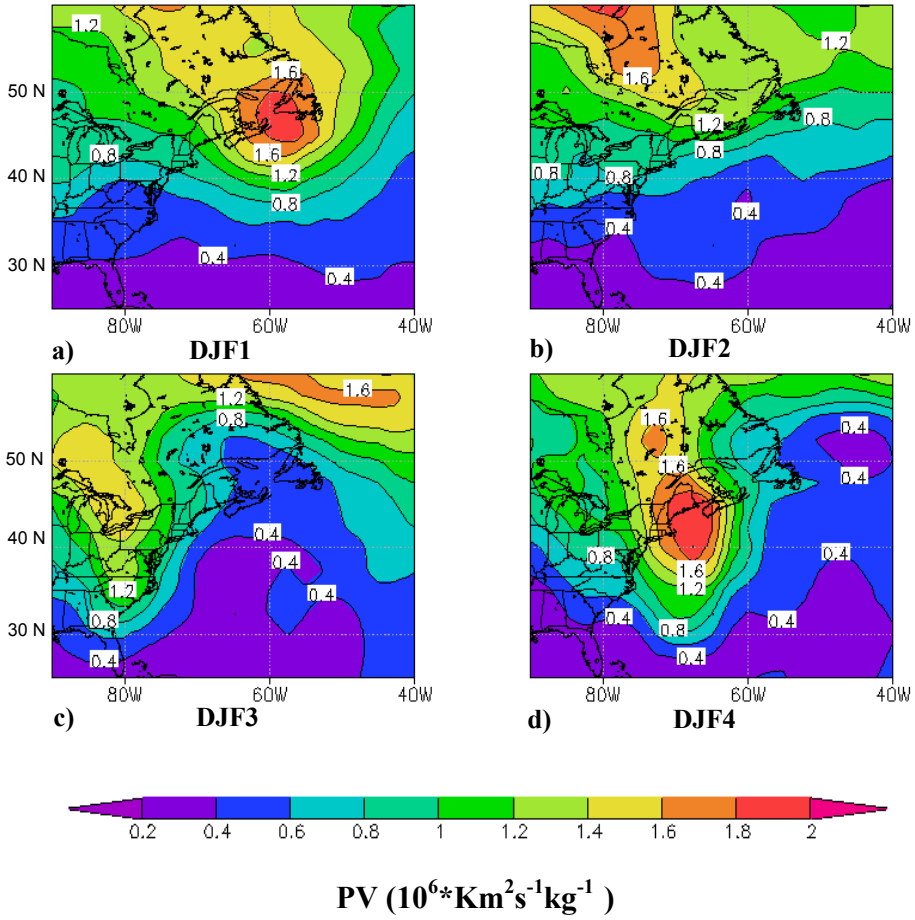

Fig. 14. NNRA potential vorticity ($10^6 \times km^2 s^{-1} kg^{-1}$) composites interpolated to 400 hPa for DJF1–DJF4 **(a–d)**.

ACPD
9, 23211–23269, 2009

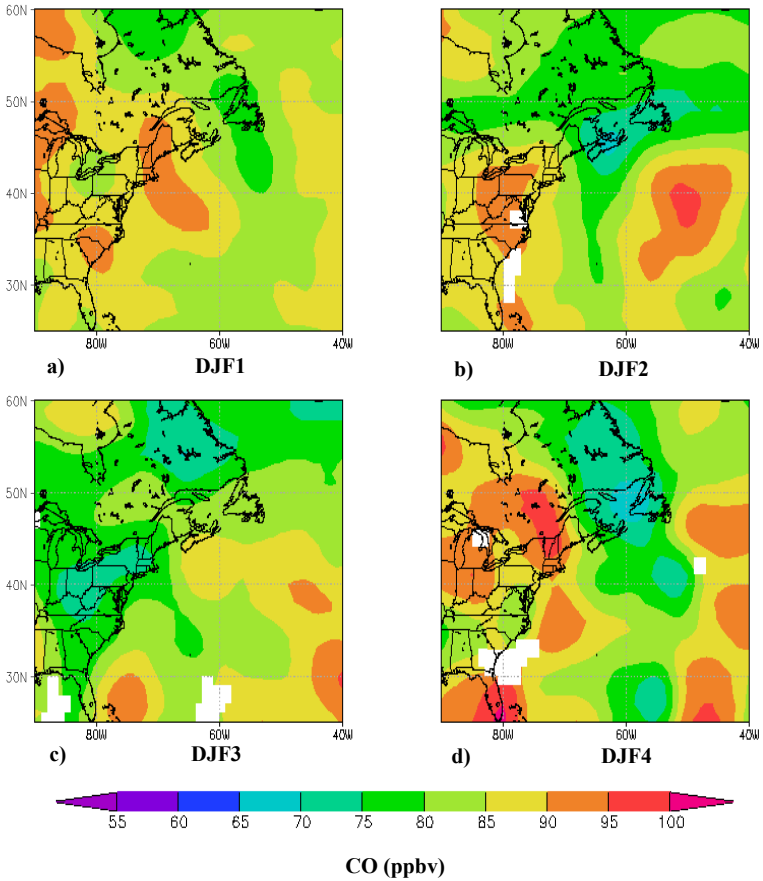

Fig. 15. The DJF 316 hPa CO (ppbv) composites for map types DJF1–DJF4 **(a–d)**.

ACPD
9, 23211–23269, 2009

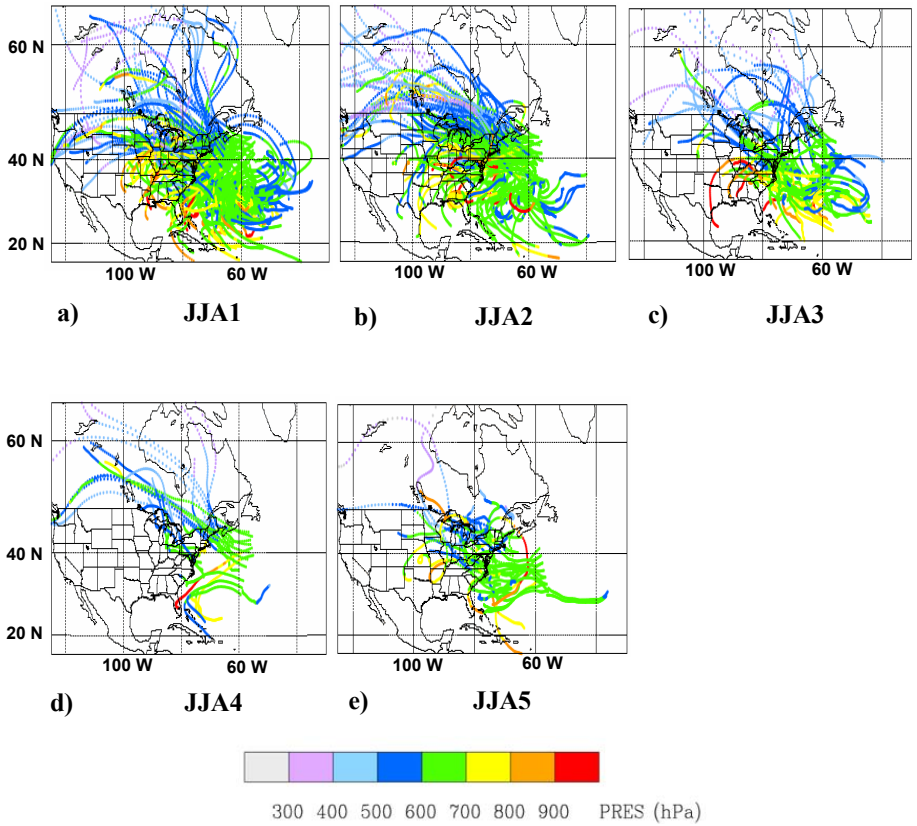

Fig. 16. Four-day HYSPLIT back trajectories using GDAS 1°×1° data from locations of TES 681 hPa observations in Region 1 for map types JJA1–JJA5 **(a–e)**. The colors indicate the pressure altitude (hPa) of the trajectory parcels.

ACPD
9, 23211–23269, 2009

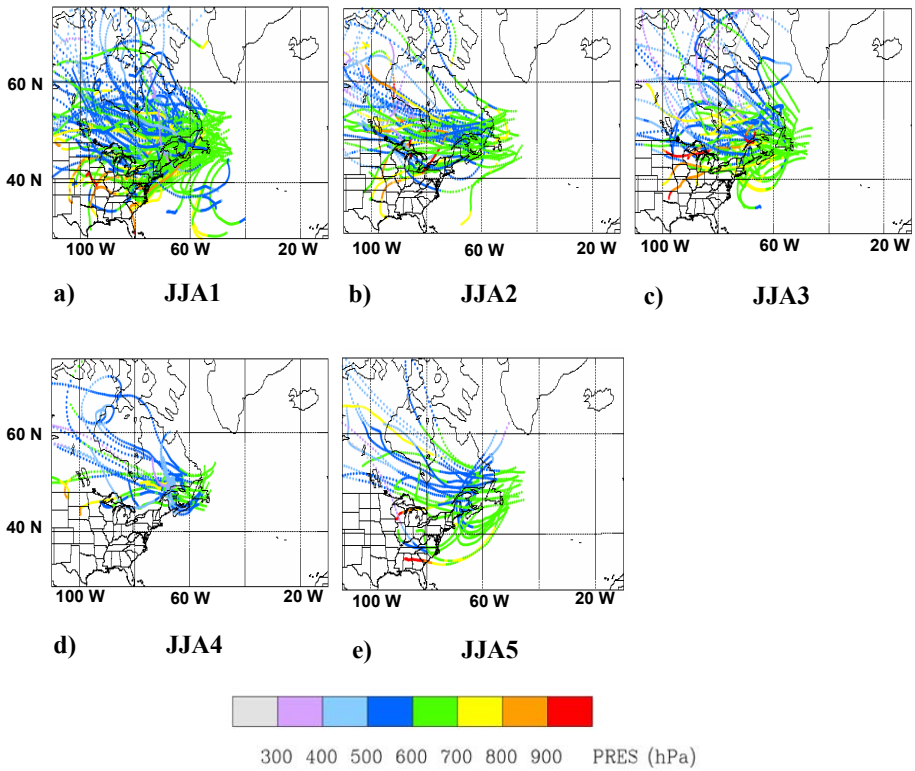

Fig. 17. Four-day HYSPLIT back trajectories using GDAS 1°×1° data from locations of TES 681 hPa observations in Region 2 for map types JJA1–JJA5 **(a–e)**. The colors indicate the pressure altitude (hPa) of the trajectory parcels.

ACPD
9, 23211–23269, 2009

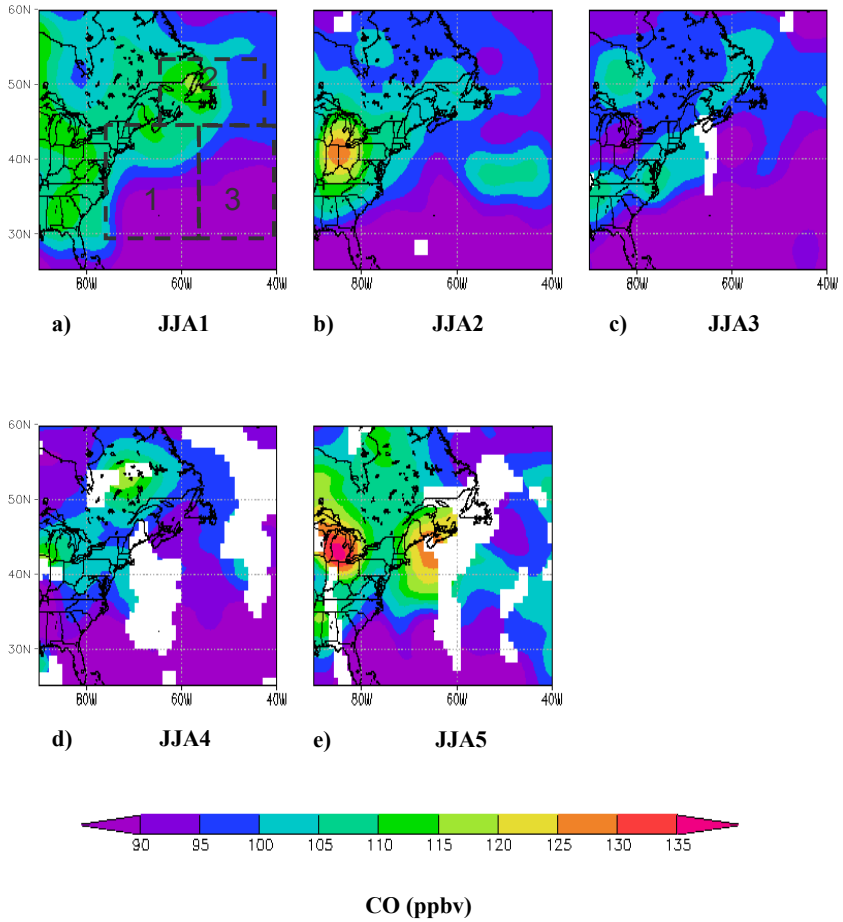

Fig. 18. The JJA 681 hPa CO (ppbv) composites for map types JJA1–JJA5 **(a–e)**.

ACPD
9, 23211–23269, 2009

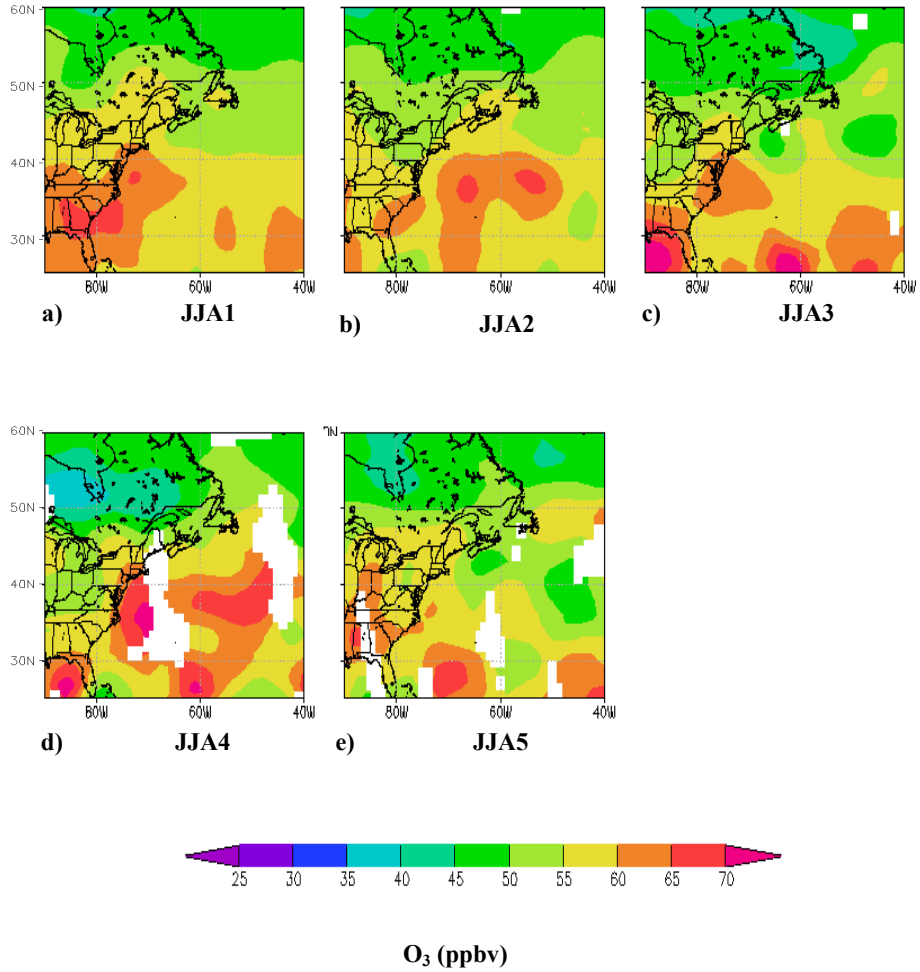

Fig. 19. The JJA 681 hPa O_3 (ppbv) composites for map types JJA1–JJA5 **(a–e)**.

ACPD
9, 23211–23269, 2009

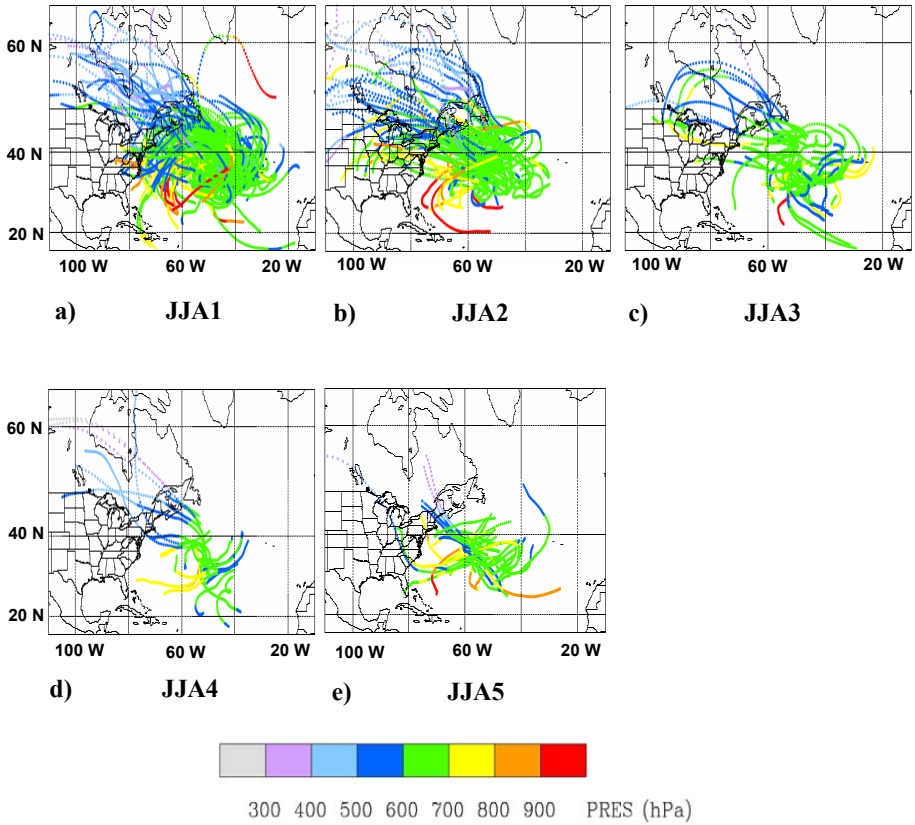

Fig. 20. Four-day HYSPLIT back trajectories using GDAS 1°×1° data from locations of TES 681 hPa observations in Region 3 for map types JJA1–JJA5 **(a–e)**. The colors indicate the pressure altitude (hPa) of the trajectory parcels.

ACPD
9, 23211–23269, 2009

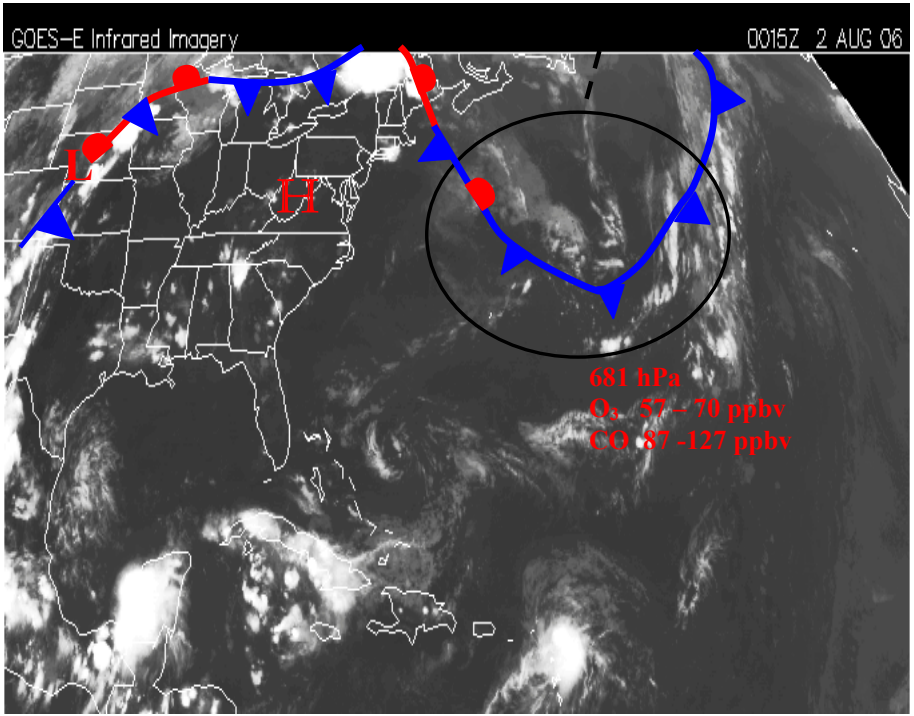

Fig. 21. GOES-East IR image for 00:15 UTC 2 August 2006 with frontal positions estimated from 00:00 UTC 1 August 2006 NCEP Atlantic surface analysis available from the National Climatic Data Center (http://www.ncdc.noaa.gov).

ACPD
9, 23211–23269, 2009

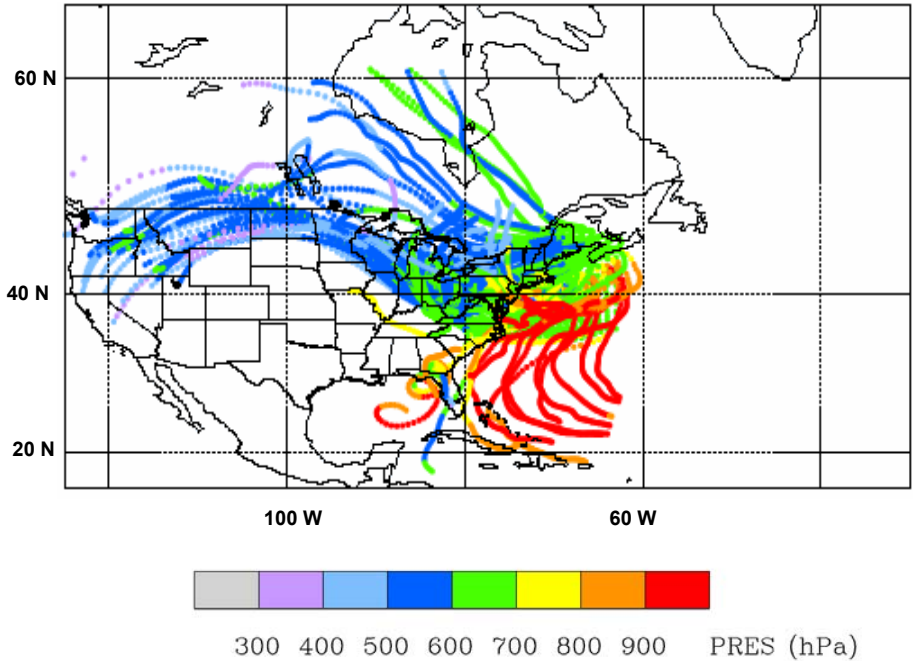

Fig. 22. HYSPLIT 4-day back trajectory matrix based on EDAS 40 km meteorological data initiated from area of enhanced 681 hPa TES CO observations at 17:00 UTC 15 June 2005. The colors indicate the pressure altitude (hPa) of the trajectory parcels.

ACPD
9, 23211–23269, 2009

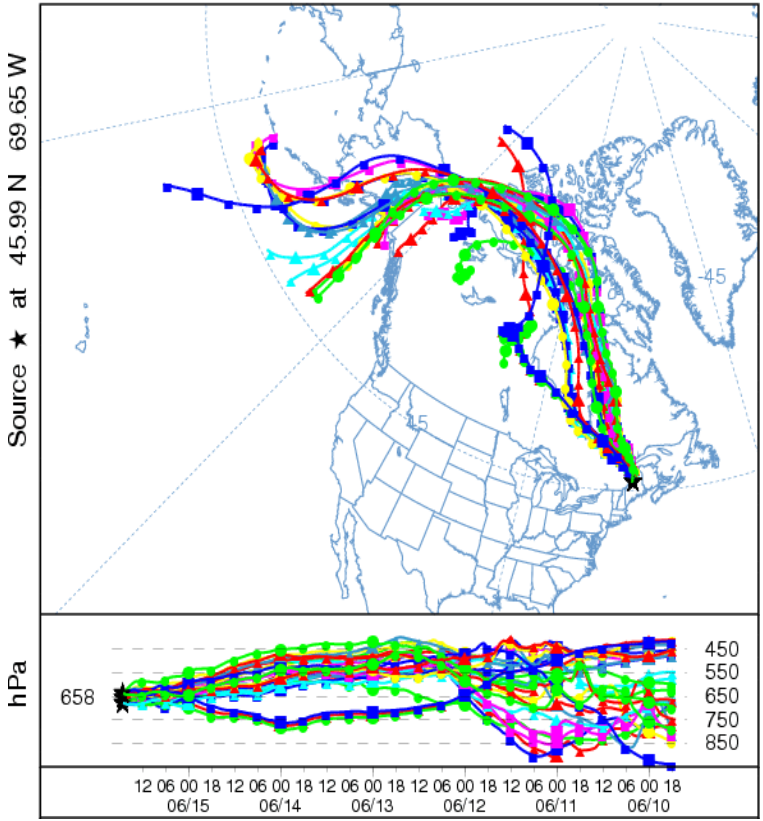

Fig. 23. HYSPLIT 5-day ensemble back trajectory based on GDAS 1°×1° meteorological data initiated from enhanced 681 hPa TES CO observation at 17:00 UTC 15 June 2005.

ACPD
9, 23211–23269, 2009